KFKI-1998-01/G
REPORT

G. Házi
G. Pór

LINEAR PHASE FORMATION BY NOISE SIMULATOR

Hungarian Academy of Sciences
CENTRAL
RESEARCH
INSTITUTE FOR
PHYSICS
BUDAPEST

KFKI-1998-01/G
REPORT

Linear Phase Formation by Noise Simulator

G. Házi[+], G. Pór[++]

[+] Simulator Laboratory (KFKI AEKI SZL) KFKI - Atomic Energy Research Institute

[++] Technical University of Budapest, Institute for Nuclear Techniques

Nomenclature and Values of Parameters

Symbol	Value	Comment
$T_c(t,z)$		temperature of coolant at height z
$T_f(t,z)$		temperature of fuel at height z
$\Phi(z)$		axial relative neutron distribution
v	$4 m/s$	velocity of coolant
$\delta t_{in}(t)$	$260 \pm 15° C$	time-dependent inlet temperature
$\overline{T}_c(t)$		average coolant temperatures over the core
$\overline{T}_f(t)$		average fuel temperatures over the core
μ_c	$5 \cdot 10^{-5}\, 1/°C$	feedback reactivity coefficients related to coolant
μ_f	$5 \cdot 10^{-6}\, 1/°C$	feedback reactivity coefficients related to fuel
ρ_{in}		constant reactivity
$\delta\rho(t)$		fluctuations of reactivity
β	0.0075	effective fraction of delayed neutrons
$\tau_c = \frac{c_{p_c}\rho_c}{h}$	$2s$	coolant time constant
$\tau_f = \frac{c_{p_f}\rho_f}{h}$	$0.1s$	fuel time constant
g	1	global weight of noise field
l	1,10,100	local weight of noise field
$\varepsilon_1 = g$	1	ex-core detector coefficient
$\varepsilon_2 = l$	1,10,100	in-core detector coefficient
h	$0.0015s$	stepsize
H	$2m$	axial length of channel
Δx	$0.003m$	length of an axial segment
S	667	number of axial segments
$\rho_s(t)$		time-dependent reactivity without fluctuations
$n(t)$		neutron level
ρ	2	Courant number for Watanabe's method

Abstract

A new, simulation technique is introduced to study noise propagation in nuclear power plants. Noise processes are considered as time functions and the dynamic behaviour of the reactor core is modelled by ordinary and partial differential equations. The equations are solved by numerical methods and the results (time series) are considered as virtual measurements. The auto power spectral density and the cross power spectral density of these time series are calculated by traditional techniques. The spectrum obtained is compared with the analytical solution to validate the new simulation approach. After validation, the simulator is expanded to investigate some physical phenomena which are unmanageable by analytical calculations. In this paper propagating disturbances are studied and the effect of non-flat flux shape on phase curves is demonstrated. Numerical problems also are briefly discussed.

Kivonat

Egy új, szimulációs technikát mutatunk be, melynek segítségével zajfolyamatok vizsgálhatók nukleáris reaktorokban. A zajfolyamatokat mint közönséges idõfüggvényeket veszük figyelmbe, a reaktorok dinamikáját pedig közönséges és parciális differenciálegyenletekkel modellezük. Az egyenleteket numerikus módszerekkel oldjuk meg és a kapott eredményeket (idõsorokat) mint a valódi méréseket dolgozzuk fel. Ezen idõsorok APSD-it és CPSD-it hagyományos módszerekkel határozzuk meg. A megszerzett spektrumokat és a származtatott mennyiségeket (fázist, koherenciát) az egyenletek analitikus megoldásaival vetjük össze, így ellenõrizve a szimulációs közelítés helyességét. Az ellenõrzés után a szimulátor alkalmas arra, hogy olyan fizikai jelenségeket vizsgáljunk segítségével, amelyek analitikus uton nem vagy csak nagy nehézségek árán kezelhetõk. Ezen jelenségek közül a terjedõ perturbációkat tanulmányozzuk, bemutatva egy valóságos axiális teljesítmény eloszlás fázisgörbékre gyakorolt hatását. Röviden tárgyaljuk azokat a numerikus problémákat is amelyek a szigorú pontossági követelményeknek köszönhetõen a felszínre kerültek.

I. Introduction

In the last few decades a number of fields of reactor diagnostics such as core barrel motion, linear phase shape between neutron (and other) detectors and the pressure waves in primary loops have been investigated [for reviews, see Kosály, 1980, Thie, 1981]. Because they have well delimited, dominant frequency regions, these fields were usually studied independently. Several models were developed to study the above mentioned physical phenomena and the experiments were interpreted by using analytical calculations. These models were modified and gradually tuned following certain physical considerations and the new models were validated again analytically or compared with real measurements. Unfortunately a complex model is often not verifiable analytically. Our eventual aim is to develop a tool that offers the possibility of testing physical theories by numerical computation. A tool of this nature is a simulator or to be more precise a 'noise simulator', which can simulate the most important physical phenomena from the point of view of noise propagation. The results in this paper were obtained using the first prototype of such a simulator. This approach based on 'pure' numerical computation is introduced to investigate disturbances propagating in nuclear power plants (NPPs). The noise sources are modelled by random number generators, the equations of the model that is used are solved in the time domain by numerical methods, and the results are processed by traditional techniques with Fast Fourier Transformation (FFT) and power spectral density (PSD) estimators, similarly to real measurements. Using this technique, investigation of complex systems and noise fields becomes possible.

Section II introduces the simple model system, which has been studied by a number of researchers analytically. Here we also give the axial positions of the detectors; these data play a significant role in the subsequent calculations. We briefly introduce the difficulties in using numerical methods to simulate noise processes in Section III. In Section IV we present our first experiments in which the well known linear phase shapes are studied by a noise simulator. Validation of the numerical methods and of the parameters are also presented in this section, comparing analytical results with numerical ones. The process of validation is presented using a flat flux profile because analytical results for the flat shape are known. Although there is considerable similarity between the analytical and simulation solutions, some differences indicate the need to analyse the results in detail. This is also done in Section IV in which we try to find a way to explain these differences. After validation, we can use the simulator to obtain new results. Contrary to earlier analytical calculations where only symmetrical flux distribution was modelled, by this technique the role of the actual flux shape can also be considered. In Section V, non-flat (real) axial flux distribution is studied.

Our future plans include extending the scope of simulation.

II. Simple Core Model for Studying Propagation of Disturbances

Disturbances that propagate axially in NPPs have been extensively studied. A simple model was studied by several authors [see for example Kosály et. al. 1977, Katona et al. 1982, Valkó 1992]. The analytical solution of this model was compared with real measurements. Although when solving the equations of this model relatively good agreement was found with the measurements, some small differences indicate the need for further investigations.
The model consists of two well-separated parts, viz. neutron kinetics and thermohydraulics. The neutron kinetics is considered by the following point model:

$$n(\omega) = G_0(\omega)\delta\rho(\omega)$$

where

$$G_0(\omega) = \frac{1}{\beta}. \tag{1}$$

It was proved by applying two-group diffusion theory (and neglecting the feedback effects) that the neutron field obeys point kinetics in the so-called 'plateau-frequency region' (0.16Hz-16Hz) for highly enriched small cores [Kosály, 1980]. Throughout this paper we assume that the point model is adequate for neutron kinetics.

Thermohydraulic processes are calculated applying a simple line kinetics model:

$$\begin{aligned} \tau_c \frac{\partial T_c(t,z)}{\partial t} &= T_f(t,z) - T_c(t,z) - v(t)\tau_c \frac{\partial T_c(t,z)}{\partial z} \\ \tau_f \frac{\partial T_f(t,z)}{\partial t} &= T_c(t,z) - T_f(t,z) + \Phi(z)n(t) \end{aligned} \tag{2}$$

The reactivity is calculated considering the temperature feedbacks as being their weighted axial temperature averages. The weights are the feedback coefficients (or reactivity coefficient of fuel and coolant correspondingly)

$$\rho_s(t) = \rho_{in}(t) + \mu_f \bar{T}_f(t) + \mu_c \bar{T}_c(t). \tag{3}$$

Although several noise sources may be considered in this model, here we are concerned solely with the effect of the reactivity and the inlet temperature fluctuations on

measurable neutron and temperature fluctuations. Both appear in the equations in the form of an additional term:

$$T_c(t,0) = T_{in}(t) + \delta T(t)$$
$$\rho(t) = \rho_s(t) + \delta\rho(t) \qquad (4)$$

Simple expressions are used to simulate the detectors and the transducers. Here, the so-called *global-local* [Kosály et al., 1977] part of the noise field is considered by weighting constants (5):

$$S_{in-core,k} = gn(t) + lT_c(t,z_k) \qquad z_k = kZ/7 \qquad k = 1..7$$
$$S_{ex-core} = \varepsilon_1 n(t) \qquad (5)$$
$$S_{ic} = \varepsilon_2 T_c(t,z)$$

The axial positions of the in-core neutron detectors are shown in Fig. 1 with an approximated real axial flux distribution. Similar distribution is observable in usual NPPs and it plays the leading role in Section V.

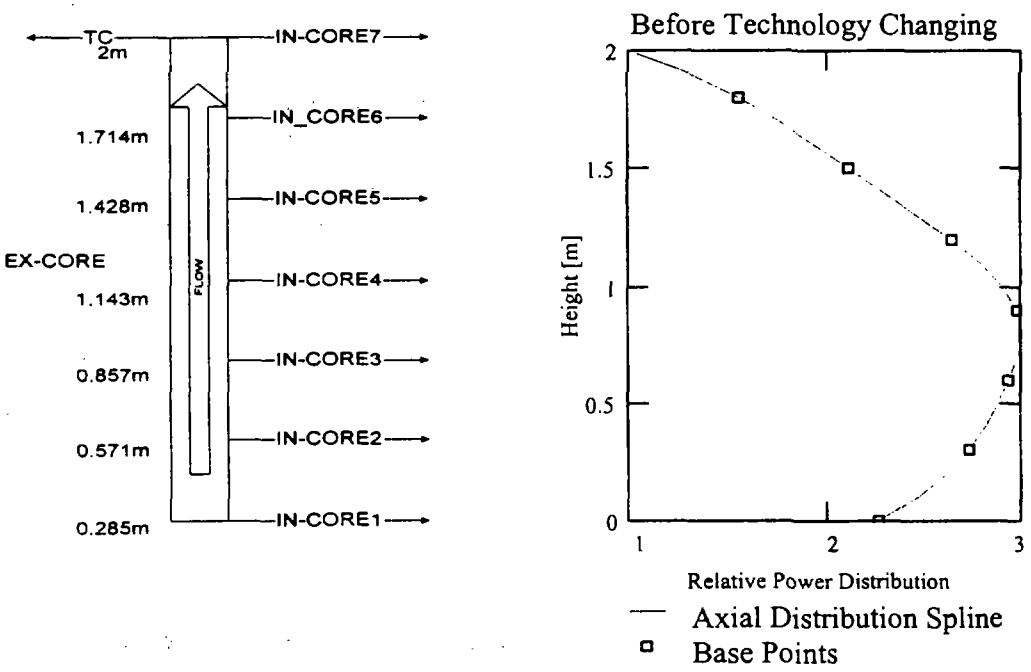

Figure 1
Axial positions of the detectors and the axial flux distribution.

III. Numerical Problems in the Frequency Domain

The equations of the model (1-4) are solved in the time domain by numerical methods, consequently the solution is an approximation.
Two problems encountered during the numerical solution are:

- the functions of the equations are noise processes and
- the solutions will be used in the frequency domain.

Why do these facts make the solution difficult ?
When a differential equation has a *white noise* function or coefficient, one must not consider this equation as an ordinary differential equation (ODE) but one should handle it like a stochastic differential equation (SDE) [Kloeden et al., 1994]. SDEs rely on a special mathematical background and on numerical solution methods. However, when a noise process is band-limited, one can consider the process as a given representation of a random process. In such a case the equations remain ODEs and traditional numerical methods are applicable. In the simulator we use band-limited noise sources and the equations are handled as deterministic equations.
Unfortunately, when one solves an ODE or a partial differential equation (PDE) the solution is not free of error. The error comes from the numerical approximation. The truncation error is due to the mathematical approach and the round-off error is caused by limited number representation of digital computers. These errors can accumulate and cause serious differences between the real and the computed solution. However, these errors are usually estimable and controllable in the time domain but not in the frequency domain. How do errors appear in the frequency domain? Maybe it has some well-definable frequency components, which falsify the results in the frequency domain.
A simple demonstration of such occurrences is presented here following Hamming [Hamming, 1962]:
Let us assume that $f(t) = e^{i\omega t}$ is a continuous function which is considered in the k-th time instant $f_k = e^{i\omega kh}$. Obviously $\frac{df_k}{dt} = i\omega e^{i\omega kh}$. Changing the differential operator by the finite difference operator, one can obtain

$$f_k' = \frac{f_{k+1} - f_{k-1}}{2h} = e^{i\omega kh}\frac{e^{i\omega h} - e^{-i\omega h}}{2h} = i\omega e^{i\omega kh}\frac{\sin \omega h}{\omega h}.$$

Thus, any frequency component is always underestimated except at 0 (DC) frequency in this approach. This example is a real problem, because finite difference techniques are often used to solve PDEs. Similarly, we point out that the numerical methods based on Taylor series (single step methods) or polynomial approach (multi step methods) can cause a serious error in the frequency domain depending on the step size and the parameters of the ODE [Házi et al. (12,13,14), 1997].

A simpler form of coolant kinetics equation is the so-called advection equation without a source term

$$\frac{\partial u}{\partial t} = -v\frac{\partial u}{\partial x}. \qquad (6)$$

This problem may also be known as a convection equation, a flux-conservative initial value problem or a first-order linear hyperbolic equation. Obviously, the solution of (6) is $u(x-vt)$. Despite being a classical problem in numerical computation, its solution remains a challenge to the experts because of a couple of properties (e.g. positivity, conservativity). Usage of the finite difference schemes usually yields numerical dissipation (from another physical viewpoint: viscosity and diffusion) and numerical dispersion [Book 1981]. It means that a wave, which should travel without any deformation along the axial axes (according to the analytical solution), will disintegrate due to the numerical dispersion (phase error), and its amplitude will decrease due to the numerical dissipation (amplitude error). Of course these side-effects are not acceptable in our approach because we need *exact* phase and amplitude information. Fortunately, there is a numerical method which can solve this equation without dissipation and dispersion, namely Watanabe's method [Watanabe, 1987]. This method is easily implementable. We tested it most carefully before using, especially from the aspect of numerical dispersion and dissipation. However, some brief notes can help to avoid unexpected difficulties. First of all, particular attention needs to be paid to the start of this method and the author's instructions should be strictly followed (though he gave no explanation why only his form of starting yields a good solution). In Watanabe's article some contradiction can be found regarding stability. Now, we should make it absolutely clear that the method is stable only when we satisfy the predetermined Courant condition, which means that the Courant number is not less than 1. Unfortunately, we often experienced numerical underflow when we wanted to use more than 1000 space segments; this seems to be the limit of the method.

The fuel kinetics equation is solved by a semidiscretized numerical scheme. Here, no special consideration is necessary because the requirements of Watanabe's method are stricter than those of the semidiscretized scheme, therefore the required segment length and step size are determined for Watanabe's method.

The noise sources were modelled by linear congruential random generators, which provide uniform distributed random numbers, in other words white noise in the frequency domain. We have mentioned that we wish to work with colour noise not with white noise. Thus the differential equations are ODEs or PDEs (not SDEs), so we have to filter the noise with a low-pass filter. We applied an 8th order elliptical low-pass filter with 10Hz cut-off frequency and 0.1dB of ripple in the pass-band and stop-band 60dB down. Because sometimes we need two noise sources at the same time, some correlation tests were accomplished between generators to avoid undesirable correlation between independent noise sources.

Finally, the time series obtained were weighted by a 256 point Hanning window and then the spectra were calculated by 50% overlapped averages.

IV. Analytical Results and Model Validation

For model validation we first have to deal with the numerical methods and their parameters. In that it seems to be a straightforward way we compare the numerical and the analytical results with each other.
The validation procedure is shown in Fig. 2.

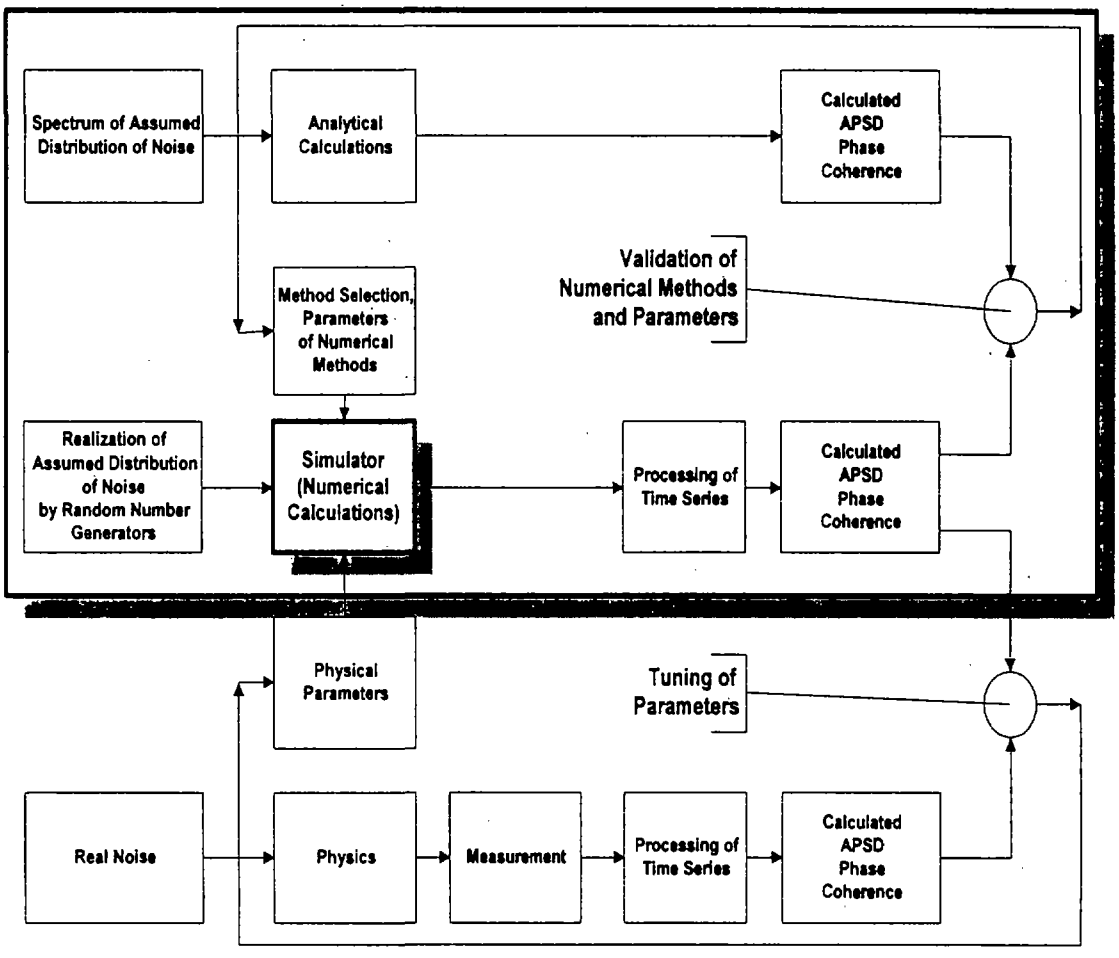

Figure 2
The process of validation. The numerical results are compared with the analytical solutions. The parameters are tuned until an acceptable resemblance is reached. After validating, real measurements are used to tune the physical parameters. This paper concentrates only on the validation of the numerical methods and parameters and does not consider the parameter validation; in other words, the upper frame in the figure is discussed.

Without going into formal proofs we give the analytical results based on calculations [Pór, 1981, Hoon, 1993].
Detector signals are defined by (5) where the power is calculated from (7)

$$P(\omega) = G_v(\omega)\left[\delta\rho(\omega) + \left[\left[\mu_f G_f(\omega) + \mu_c\right] Y(\omega, H)\delta T_{in}(\omega)\right]\right] \tag{7}$$

the coolant temperature is obtained from (8)

$$T_c(\omega, z) = \delta T_{in}(\omega)\left[e^{-i\frac{\omega}{v}z} + \frac{q}{v\tau_c} G_f(\omega) z Y(\omega, z) G_v(\omega)\left[\mu_f G_f(\omega) + \mu_c\right] Y(\omega, H)\right] +$$
$$+\delta\rho(\omega)\frac{q}{v\tau_c} G_f(\omega) z Y(\omega, z) G_v(\omega) \tag{8}$$

where the following transfer functions are applied:

$$G_f(\omega) = \frac{1}{1 + i\omega\tau_f},$$

$$Y(\omega, z) = e^{-\frac{i\omega z}{2v}} \frac{\sin\frac{\omega z}{2v}}{\frac{\omega z}{2v}}, \tag{9}$$

$$G_v(\omega) = \frac{1}{\frac{1}{G_0} - \left(\mu_f G_f(\omega) + \mu_c\right)\frac{q}{i\omega\tau_c} G_f(\omega)\left[1 - Y(\omega, H)\right] - \mu_c G_f(\omega) q}.$$

Two independent noise sources (reactivity and inlet temperature) and their combination are investigated both analytically and numerically (by the simulator) for three different global/local ratios. All phase curves are shown in App. II, which is divided into three parts based on the combination of noise sources.

The curves in App. II were produced by applying an atan(...) function instead of an arg(...) function (this function corresponds to the well-known atan2(...) function), which considers the sign of the real and the imaginary part of the CPSD. The reason why we applied the atan(...) function was clarified by Valkó [Valkó, 1992]. He drew attention to the arg(...) function that can produce undesirable 180 degree phase jumps in the phase curves. This effect is shown in Fig. 3.

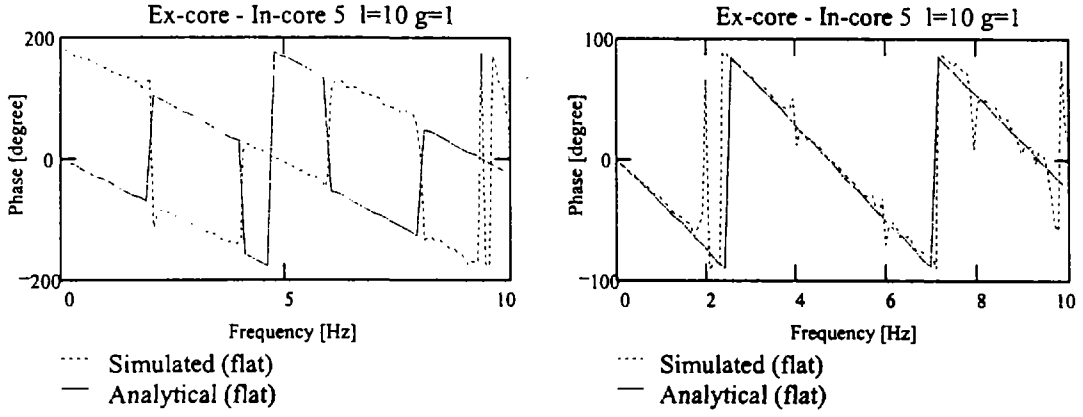

Figure 3

The phase between the ex-core and the in-core detectors is shown applying two different phase functions. The phase on the left was obtained by applying an arg(...) function. Here 180 degree phase jumps are noticeable due to the undesirable effect of the arg(...) function. On the right hand side the phase was calculated by using a simple atan(...) function. This phase is free of phase jumps and the phase is very close to the analytical result.

The phase jumps coming from the arg(...) function are easily explainable for sink functions. Let us investigate a simple transfer function, which changes the sign of the real part of the transfer function at all sink frequencies:

$$H(\omega) = \frac{\sin(\omega)}{\omega}$$

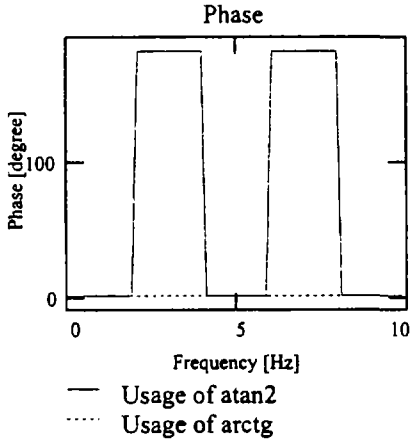

Figure 4

Phase shift of sin(x)/x function using atan(...) and arg(...) functions. The arg(...) function causes 180 degree phase jumps at sink frequecies.

The arg(...) function is sensitive to sign changing and it produces 180 degree phase jumps here. Thus, although the atan(...) function does not consider the sign of the real and imaginary part we apply this instead of the other because we wish to concentrate on the differences due to the simulation.

Let us now consider *reactivity noise only.* If one looks at the analytical and the numerical results a strong similarity is observable. However, some small differences indicate that the phase curve in Fig. 5 be viewed painstakingly whereupon some minor differences at 2, 4, 6, 8Hz may be realized.

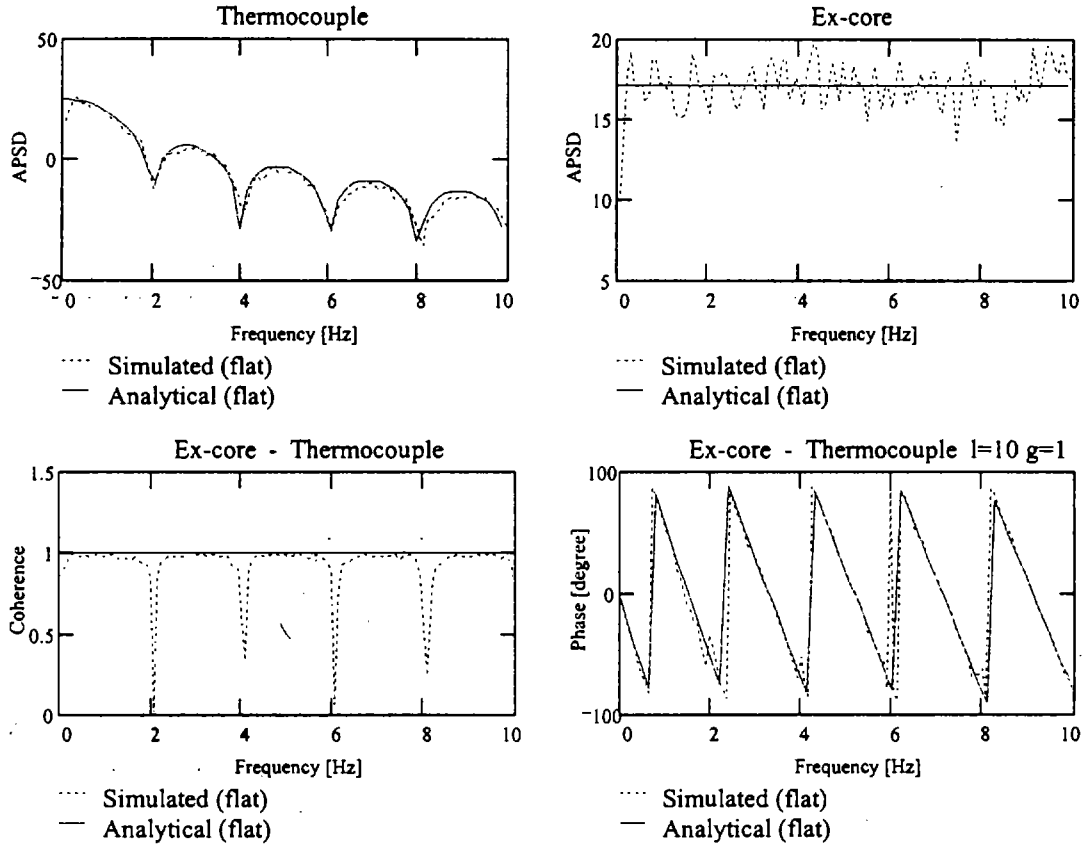

Figure 5

APSDs, coherence and phase functions are shown for thermocouple and ex-core detectors. The global-local ratio was 10. Although a good agreement can be found, some details indicate that the investigations be continued.

Some small peaks (at 2, 4, 8Hz) and a large peak (at 6Hz) appear in the curve, that do not exist in the case of analytical calculations. These peaks appear precisely at the sink frequencies, where the coherence function also has deep sinks. Because the calculation resulted from only one noise source, the coherence function should be equal to one for all frequency components except if there is another noise source.

Similar problems appear for other detector combinations. Spectra from two in-core detectors at different axial positions are considered and shown in Fig. 6.

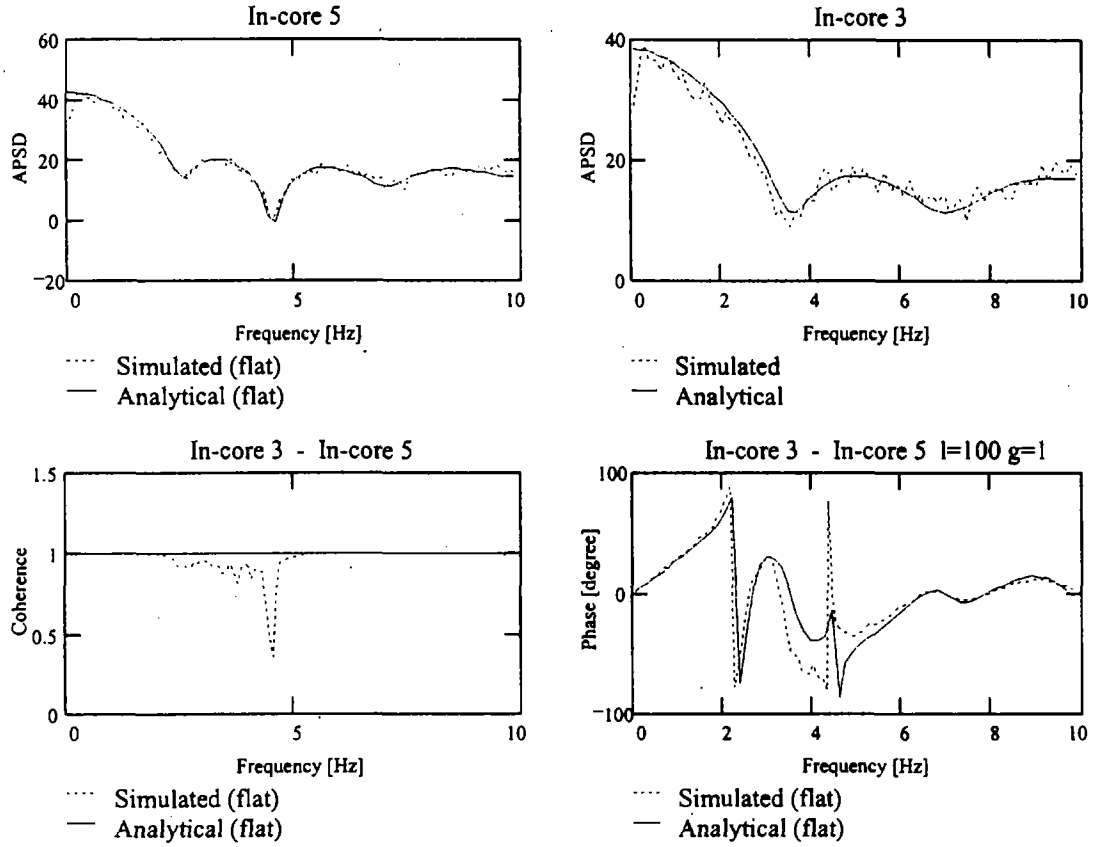

Figure 6

APSDs, coherence and phase functions are shown for two in-core detectors.. The coherence function decreases in the frequency region 2-6Hz, and there are some deviations in the phase curve also. The local-global ratio is equal to 100.

There are some deviations from the analytical solution in the frequency region of 2-6Hz in the simulation results. Since the phases were obtained from the power spectra estimations, we should first be convinced that the estimations are accurate. The coherence functions provide a direct indication of the error of the estimation. If the coherence function has low values in a given frequency region, the phase curves cannot be good, because it means that the estimation has a large statistical error. Thus the question arises: What is the reason for the decrease of the coherence at the sink frequencies ? We shall consider this deviation in App. I.

V. Effect of Non-Flat Flux Shape on the Phase Curves

On the basis of our original aim we investigated the effect of a realistic flux shape on the phase function estimation using the simulation technique. We would again mention that this is not estimatable by using analytical expressions. In App. II of this report, phase pictures are given for several different combinations, and differently placed neutron and temperature detectors. Here we draw attention to some well selected cases only.

a. Single reactivity noise source

In some cases (like ex-core - in-core combinations, see Fig. 7; and thermocouple cases, see App. II) one can see (Fig. 7) that a realistic flux shape leads to larger local effect. This is well understandable in spite of the fact that the *local-global* ratio was kept to its earlier value because the integral of the flux weighted global part became smaller (the entire proof and the interpretation of this integral is given for instance in [Pór, 1981]).

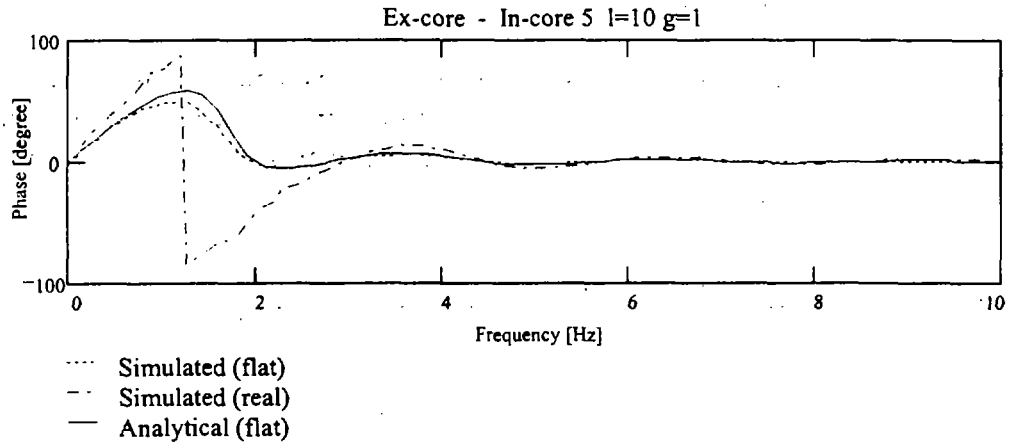

Figure 7
Phase between ex-core and in-core 5 detectors.

In the case of in-core - in-core combinations the deviance from the single global and local concept is large: between 2 and 4Hz even in the flat flux case (see Fig. 8). Realistic flux leads to even more complicated structure in that frequency region. Our conclusion was that only the low frequency range can be used for simple velocity parameter estimation. However, this simulation can explain several strange phases observed earlier in certain measurements [Pór et. al. 1997].

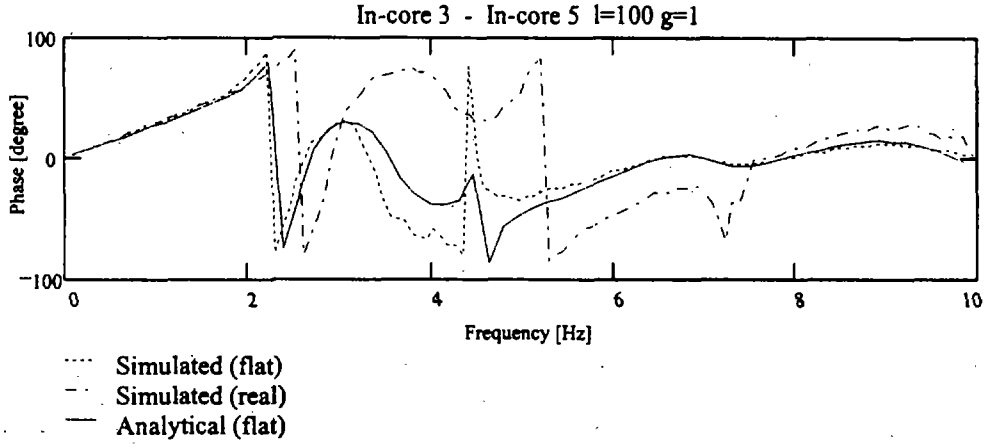

Figure 8

Phase between in-core 3 and in-core 5 detectors.

b. Single inlet temperature noise source

Figure 9 proves that a more realistic flux shape leads to a substantial change in the slope of the phase function. This is a very important conclusion since it means that a velocity estimation based on a model with a simple flat flux approximation can mislead us and can cause a biased estimation of the velocity.

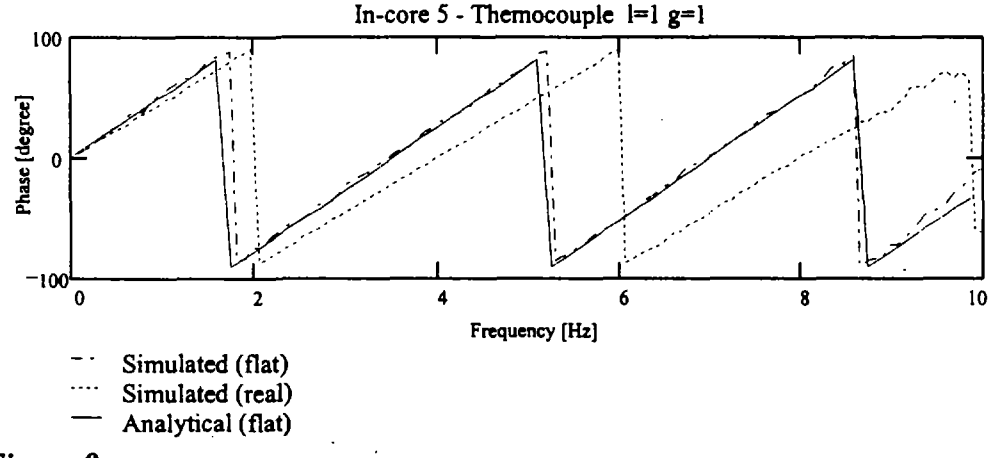

Figure 9

Phase between in-core 5 and thermocouple detectors.

c. Combined noise sources

Unfortunately the two conclusions above are not valid in every case. When we applied a combined input noise source we got a contradictory result. In Fig. 10/a the phase between an in-core neutron detector and thermocouple is shown for a single reactivity noise source. This phase coincides with the results of Section V.a. In Fig. 10/b the phase estimation for the same detector combination is shown for a single inlet temperature noise source. This phase also coincides with the results of Section V.b. Figure 10/c shows the

combined noise sources effect on phase. Here, the effect of realistic flux shape is negligible, we cannot observe the combination of the above mentioned effects. In view of this, further investigations are planned.

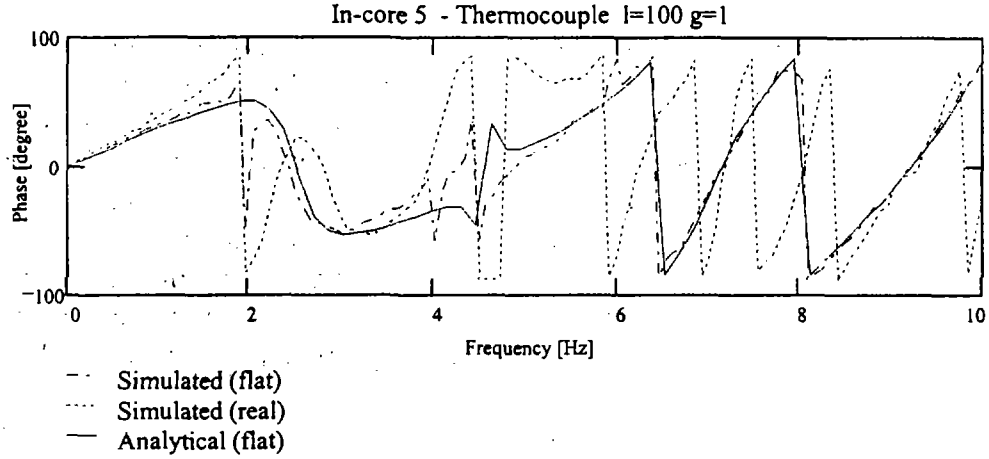

Fig. 10/a

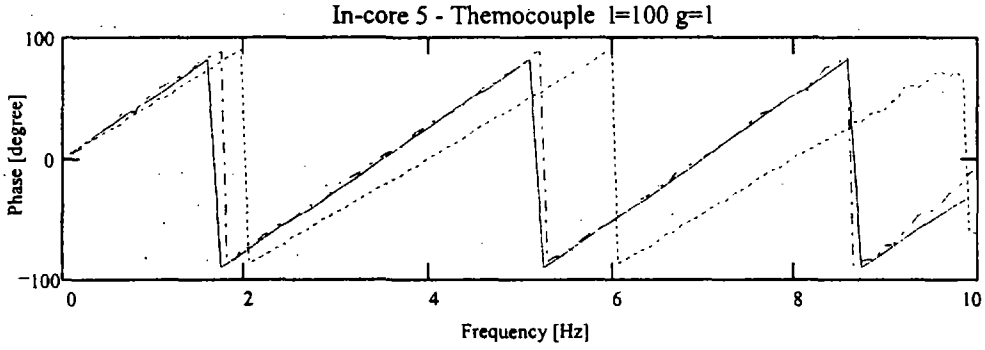

Fig. 10/b

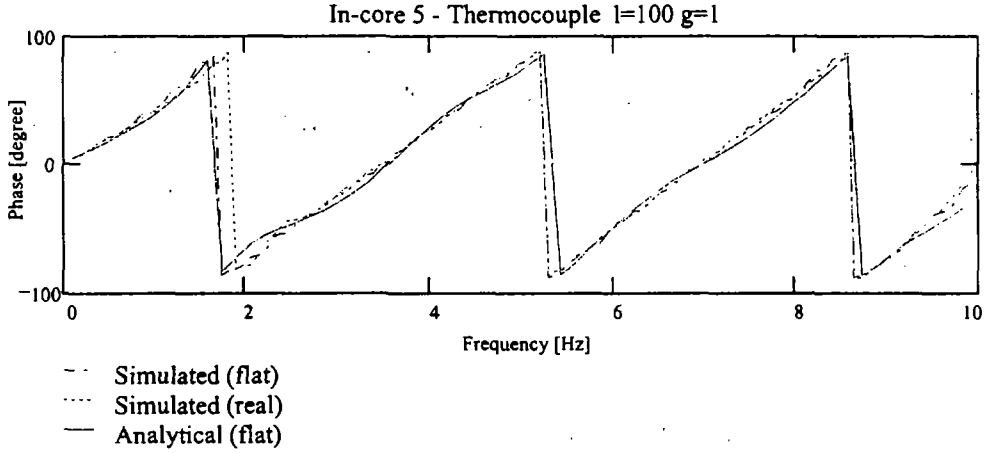

Fig. 10/c

Figure 10

Phase between in-core 5 and thermocouple detectors for single reactivity noise (10/a), for single inlet temperature noise (10/b), and for combinations of both noise sources (10/c).

VI. Conclusions and Future Plans

We have completed the development of the first prototype of a noise simulator. Our initial results show that the application of a simulator of this kind will help towards understanding more details of real measurements. The effect of a realistic flux shape on phase curves was briefly introduced. Some conclusions related to this field were mentioned in the previous section. Our results indicate the need to continue the investigations by running the simulator with variable physical parameters and flux shapes. We intend to carry out more simulations using the same programming package but with different flux shapes and different reactor parameters, we shall mainly vary the velocity and the *local-global* ratio with the aim of producing a training set which could be used for training neural networks.
It is, however, emphasized that the development of models should be continued. It would appear that a more sophisticated model (3-dimensional diffusion model with 3-dimensional thermohydraulic model) might well lead to several worthwhile results.

Acknowledgement

The authors wish to express their gratitude to the KFKI Atomic Energy Research Institute (KFKI AEKI) as a whole and to the staff of KFKI AEKI's Simulator Laboratory for their unstinting advice throughout the investigations. The authors particularly wish to thank Mr. J.S. Jánosy.

Appendix I

Strangeness of Coherence and Phase Functions

First of all one has to consider that the roundoff error of numerical methods corresponds to an inevitable noise source. Let us analyse this situation.
One can obtain the measured (or numerically computed) signals based on correlation (5) for different types of detectors:

$$\begin{aligned} S_{in-core,k}(\omega) &= H_{in-core}(\omega)\delta\rho(\omega) \\ S_{ex-core}(\omega) &= H_{ex-core}(\omega)\delta\rho(\omega) \\ S_{ic}(\omega) &= H_{ic}(\omega)\delta T(\omega) \end{aligned} \qquad (10)$$

where the transfer functions are the following:

$$H_{in-core}(\omega) = gG_v(\omega) + l\frac{q}{v\tau_c}G_f(\omega)z_k Y(\omega, z_k)G_v(\omega)$$
$$H_{ex-core}(\omega) = \varepsilon_1 G_v(\omega) \qquad (11)$$
$$H_{ic}(\omega) = \varepsilon_2 l\frac{q}{v\tau_c}G_f(\omega)HY(\omega, H)G_v(\omega)$$

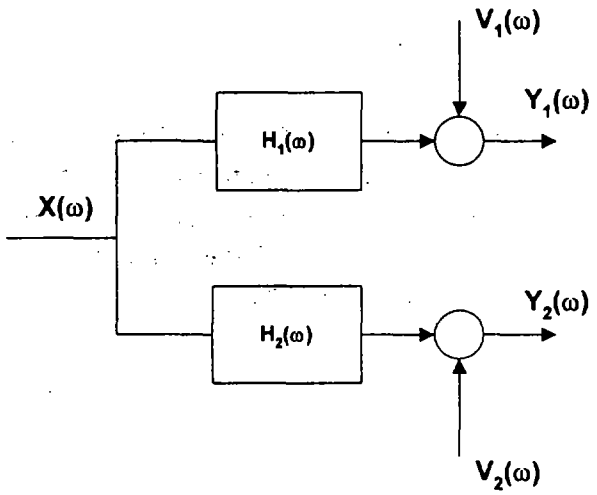

Figure 11.
One input and two output system with additive coherent noise members in the outputs.

The coherence between two detectors is equal to one in linear systems if there is only one noise source in the system.

$$\gamma^2(\omega) = \frac{CPSD_{Y_1Y_2}(\omega)CPSD_{Y_1Y_2}(\omega)^*}{APSD_{Y_1}(\omega)APSD_{Y_2}(\omega)} = \frac{|H_1(\omega)|^2|H_2(\omega)|^2 APSD_X^2(\omega)}{|H_2(\omega)|^2|H_1(\omega)|^2 APSD_X^2(\omega)} = 1. \qquad (12)$$

Although our system was a linear one and we studied the system using only one excitation source, the coherence functions were far from the theoretical hopes. This behaviour is due to the following transfer function,

$$Y(\omega, z) = e^{-\frac{i\omega z}{2v}}\frac{\sin\frac{\omega z}{2v}}{\frac{\omega z}{2v}} \qquad (13)$$

which is quite different from the usual fractional rational functions. Appearance of a transcendent transfer function leads to an input-output relation where the input signal has limited energy whereas the output signal has none at the defined frequencies.

$$\omega = \frac{4k\pi v}{z} \rightarrow H_{in\sim core,k}(\omega) = gG_v(\omega)$$
$$\omega = \frac{4k\pi v}{H} \rightarrow H_{tc\sim core}(\omega) = 0 \tag{14}$$

Let us look at Fig. 11., where $y_1(t), y_2(t)$ correspond to signals of any detector type, $x(t)$ is considered as any input noise, and $H_1(\omega), H_2(\omega)$ are transfer functions related to any corresponding output signal to be measured. We shall consider additive white noise sources for each detector signal because the numerical results surely have roundoff errors. The output signals are the superposition of the noise and the signal terms.

$$Y_1(\omega) = H_1(\omega)X(\omega) + V_1(\omega)$$
$$Y_2(\omega) = H_2(\omega)X(\omega) + V_2(\omega) \tag{15}$$

Taking into account that $X(\omega)$ is independent of $V_1(\omega), V_2(\omega)$ and that both output noise sources are correlated one can obtain the cross-spectral density between the detectors

$$CPSD_{Y_1Y_2}(\omega) = H_1(\omega)H_2^*(\omega)APSD_X(\omega) + CPSD_{V_1V_2}(\omega) \tag{16}$$

The auto-spectral densities are easily obtained for each detector based on the following relations

$$APSD_{Y_1}(\omega) = |H_1(\omega)|^2 APSD_X(\omega) + APSD_{V_1}(\omega)$$
$$APSD_{Y_2}(\omega) = |H_2(\omega)|^2 APSD_X(\omega) + APSD_{V_2}(\omega) \tag{17}$$

Considering correlated output noises due to the roundoff of numerical computation the coherence function (18) may be far from the real one

$$\gamma^2(\omega) = \frac{CPSD_{Y_1Y_2}(\omega)CPSD_{Y_1Y_2}(\omega)^*}{APSD_{Y_1}(\omega)APSD_{Y_2}(\omega)} = \tag{18}$$
$$= \frac{\left(H_1(\omega)H_2^*(\omega)APSD_X(\omega) + CPSD_{V_1V_2}(\omega)\right)\left(H_1(\omega)H_2^*(\omega)APSD_X(\omega) + CPSD_{V_1V_2}(\omega)\right)^*}{\left(|H_1(\omega)|^2 APSD_X(\omega) + APSD_{V_1}(\omega)\right)\left(|H_2(\omega)|^2 APSD_X(\omega) + APSD_{V_2}(\omega)\right)}$$

The most interesting case is when one of the studied detectors is the thermocouple. Here, in an analytical case, the cross-spectral density and the auto-spectral density become zero at $\omega_{TCs} = 4k\pi v/H$ frequencies due to the sink function in (11), because here

$$H_{ic}(\omega_{TCs}) = 0 \tag{19}$$

and the coherence function (16) will be calculated from the 0/0 ratio.
In the numerical case the coherence function between a thermocouple and any other detector comes from (18), which one can simplify to (20) based on (19) at sink frequencies

$$\gamma_{TC...}^{2}(\omega_{TCs}) = \frac{\left|CPSD_{V_1V_2}(\omega_{TCs})\right|^2}{APSD_{V_1}(\omega_{TCs})\left(\left|H_2\right|^2 APSD_X(\omega_{TCs}) + APSD_{V_2}(\omega_{TCs})\right)} \tag{20}$$

Here the coherence depends on the input signal power, the power of the output noises, and the correlation between output signals. Needless to say that taking account of uncorrelated roundoff errors the numerator of (20) becomes zero

$$CPSD_{V_1V_2}(\omega_{TC_s}) = 0,$$

in other words, in this case the coherence is also equal to zero.
The effect of sink structure on the coherence function is less for ex-core - in-core and in-core - in-core detector combinations than thermocouples because these signals have finite energy for each component due to the power term. Thus the coherence value is higher at sink frequencies for the combination of such kind of detectors than the combination of thermocouple and any other kind of detector.

Appendix II

This appendix contains the phase curves obtained

- for reactivity noise,
- for inlet temperature noise,
- and for combinations of reactivity and inlet temperature noise.

All figures have three curves in accordance with the flat flux analytical formula (5), with the simulated series with flat flux shape, and with the simulated time series with realistic flux shape.

Phase Curves for Reactivity Noise

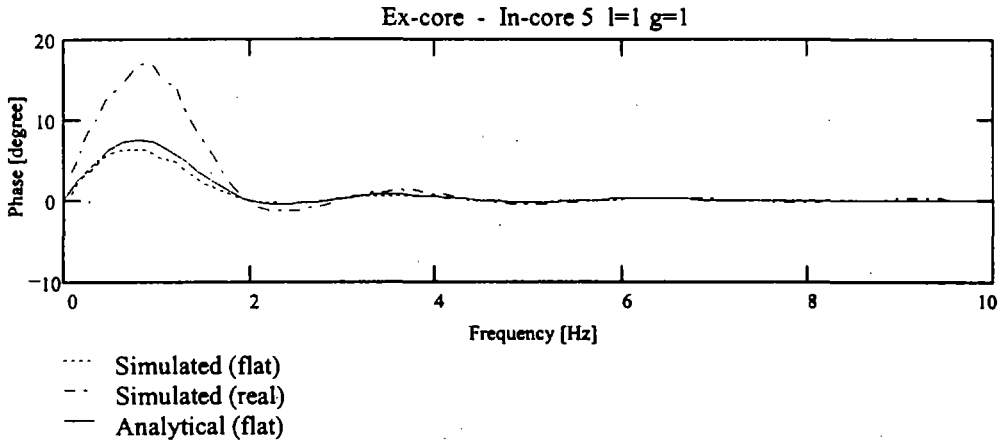

A1

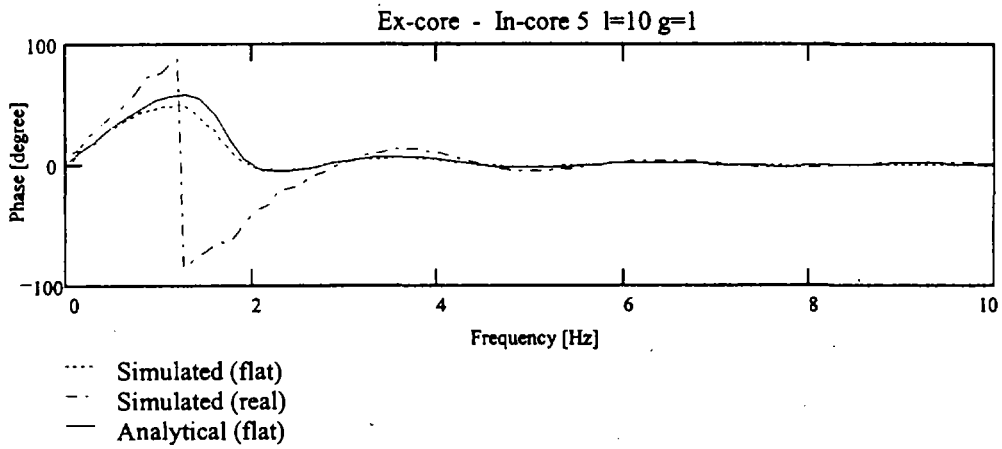

A2

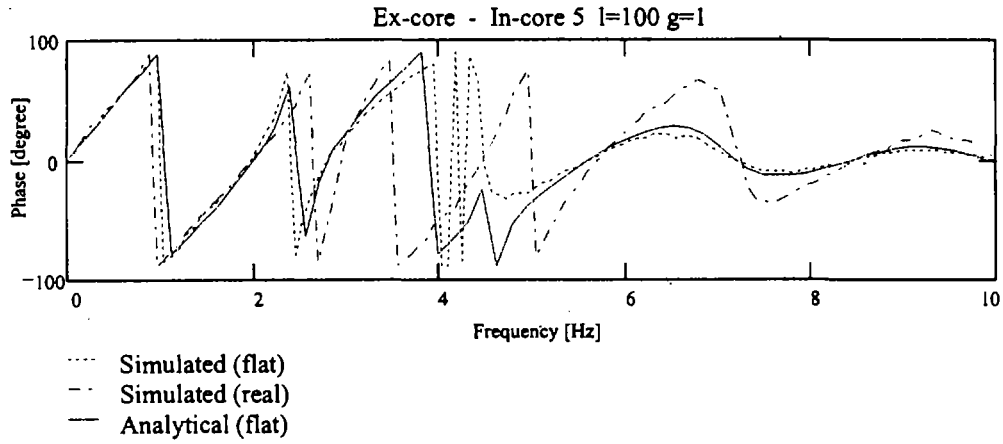

A3

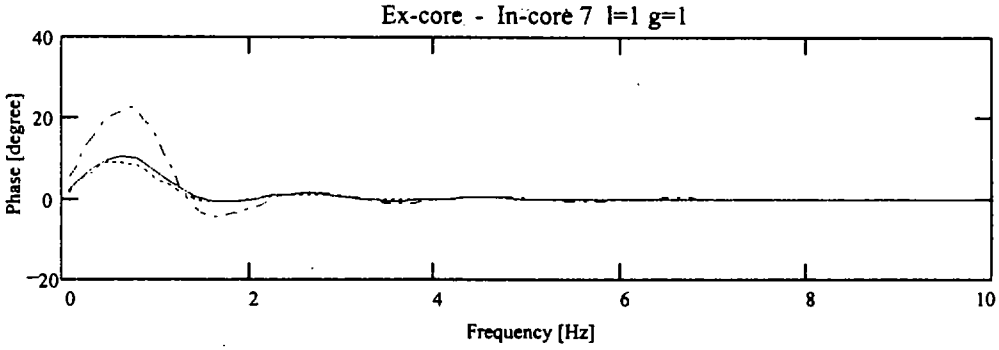
Ex-core - In-core 7 l=1 g=1
Phase [degree]
40
20
0
-20
0
2
4
6
8
10
Frequency [Hz]
Simulated (flat)
Simulated (real)
Analytical (flat)

A4

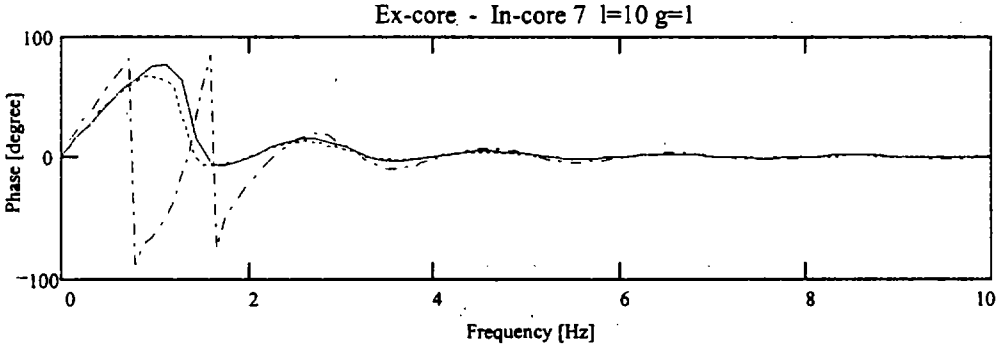
Ex-core - In-core 7 l=10 g=1
Phase [degree]
100
0
-100
0
2
4
6
8
10
Frequency [Hz]
Simulated (flat)
Simulated (real)
Analytical (flat)

A5

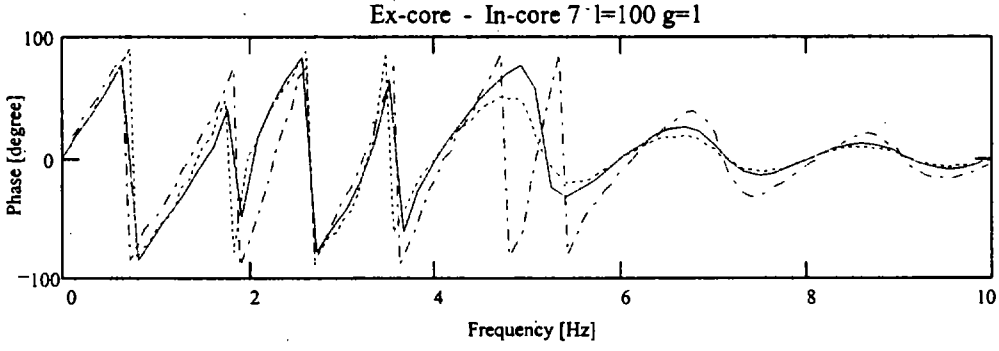
Ex-core - In-core 7 l=100 g=1
Phase [degree]
100
0
-100
0
2
4
6
8
10
Frequency [Hz]
Simulated (flat)
Simulated (real)
Analytical (flat)

A6

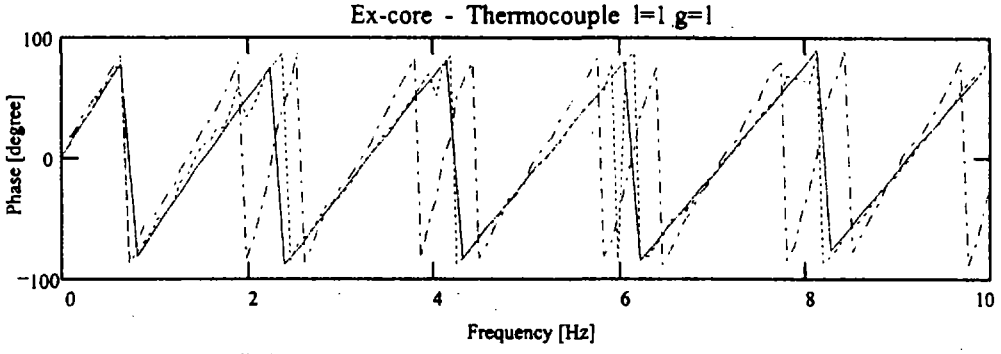
Ex-core - Thermocouple l=1 g=1
Phase [degree]
100
0
-100
0
2
4
6
8
10
Frequency [Hz]
Simulated (flat)
Simulated (real)
Analytical (flat)

A7

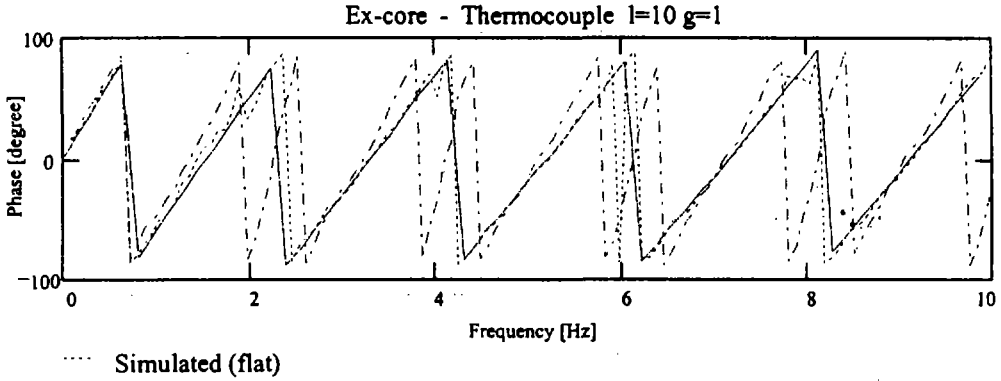
Ex-core - Thermocouple l=10 g=1
Phase [degree]
100
0
-100
0
2
4
6
8
10
Frequency [Hz]
Simulated (flat)
Simulated (real)
Analytical (flat)

A8

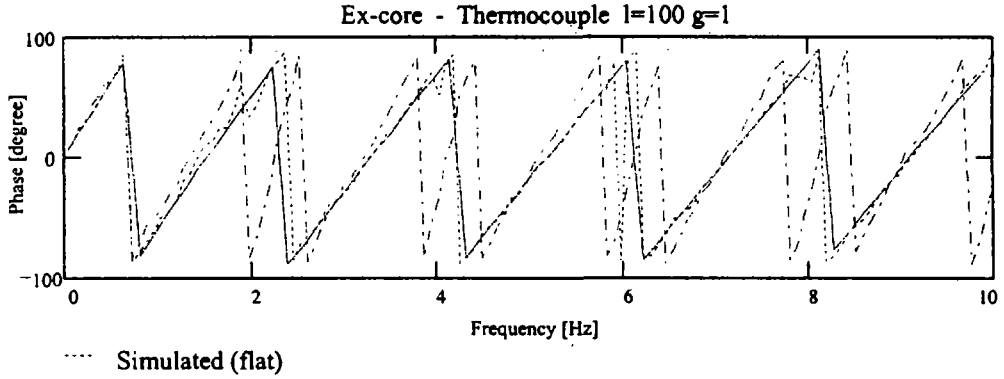
Ex-core - Thermocouple l=100 g=1
Phase [degree]
100
0
-100
0
2
4
6
8
10
Frequency [Hz]
Simulated (flat)
Simulated (real)
Analytical (flat)

A9

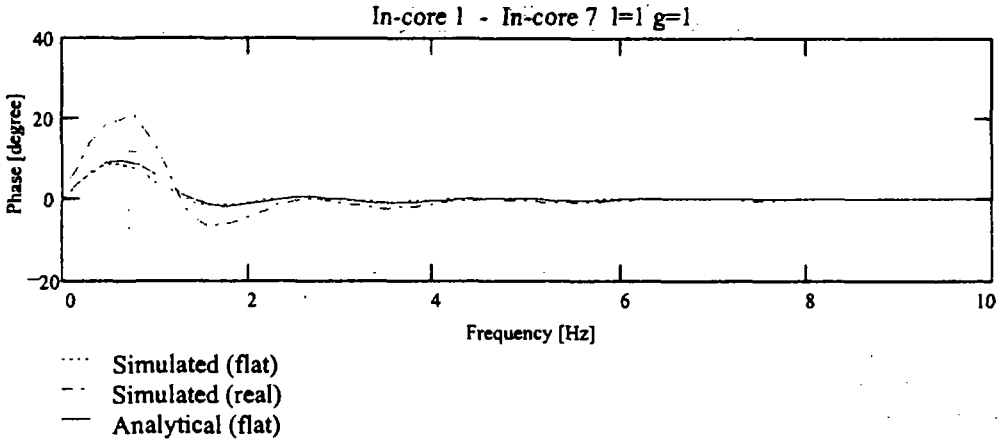
In-core 1 - In-core 7 l=1 g=1
Phase [degree]
Frequency [Hz]
Simulated (flat)
Simulated (real)
Analytical (flat)

A10

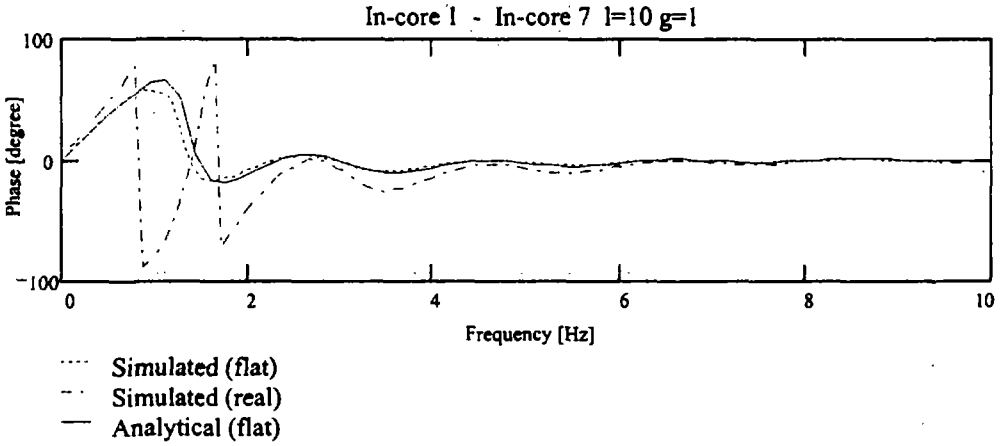
In-core 1 - In-core 7 l=10 g=1
Phase [degree]
Frequency [Hz]
Simulated (flat)
Simulated (real)
Analytical (flat)

A11

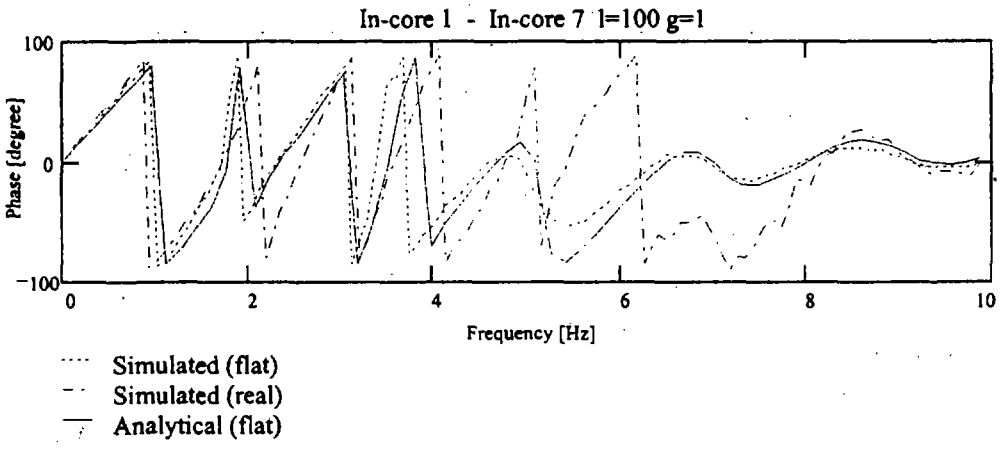
In-core 1 - In-core 7 l=100 g=1
Phase [degree]
Frequency [Hz]
Simulated (flat)
Simulated (real)
Analytical (flat)

A12

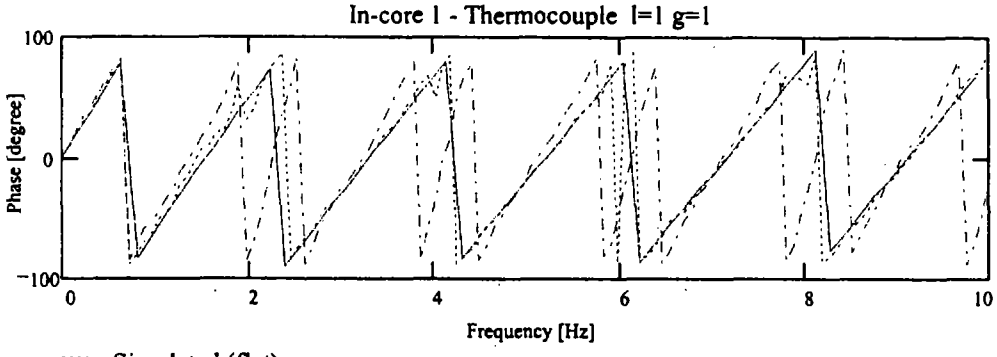
In-core 1 - Thermocouple l=1 g=1
Phase [degree]
100
0
-100
0
2
4
6
8
10
Frequency [Hz]
Simulated (flat)
Simulated (real)
Analytical (flat)

A13

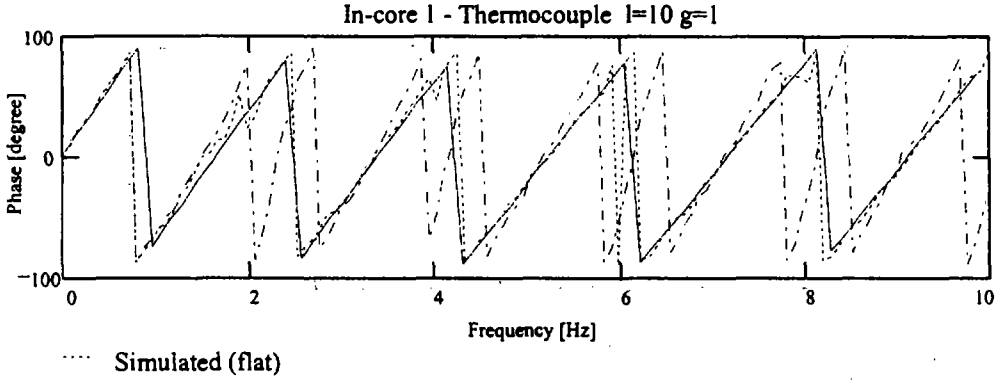
In-core 1 - Thermocouple l=10 g=1
Phase [degree]
100
0
-100
0
2
4
6
8
10
Frequency [Hz]
Simulated (flat)
Simulated (real)
Analytical (flat)

A14

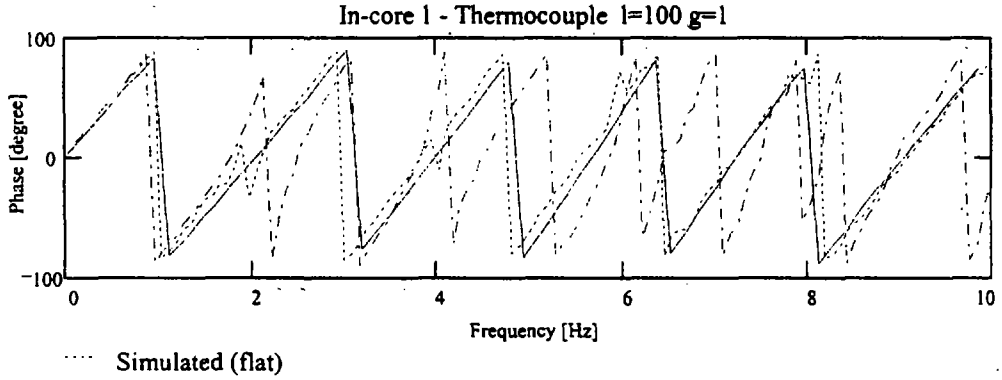
In-core 1 - Thermocouple l=100 g=1
Phase [degree]
100
0
-100
0
2
4
6
8
10
Frequency [Hz]
Simulated (flat)
Simulated (real)
Analytical (flat)

A15

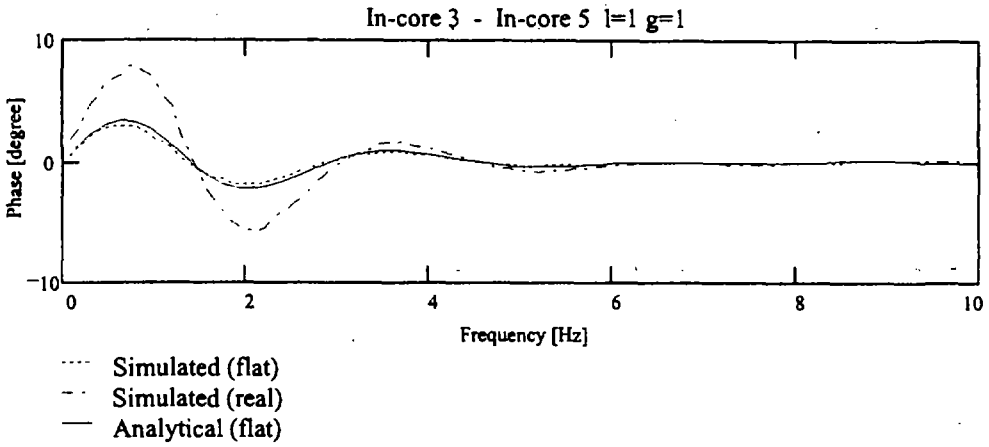
In-core 3 - In-core 5 l=1 g=1
Phase [degree]
10
0
−10
0
2
4
6
8
10
Frequency [Hz]
Simulated (flat)
Simulated (real)
Analytical (flat)

A16

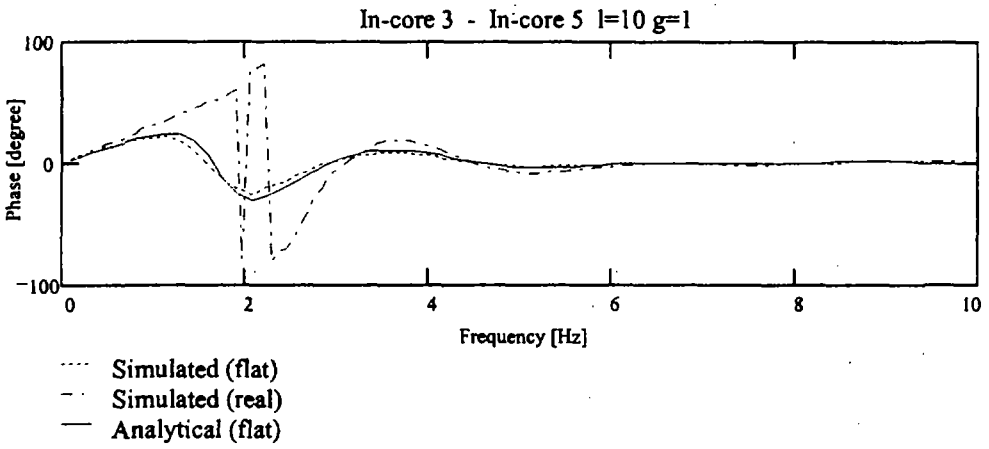
In-core 3 - In-core 5 l=10 g=1
Phase [degree]
100
0
−100
0
2
4
6
8
10
Frequency [Hz]
Simulated (flat)
Simulated (real)
Analytical (flat)

A17

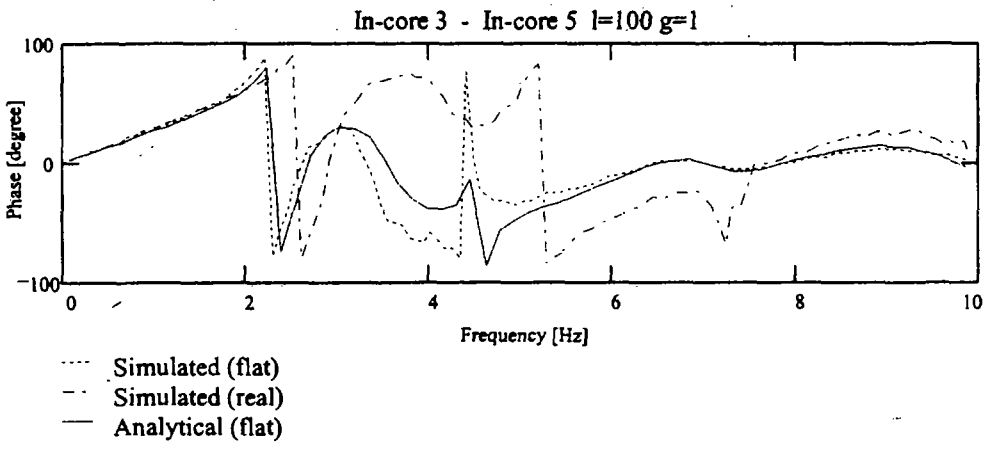
In-core 3 - In-core 5 l=100 g=1
Phase [degree]
100
0
−100
0
2
4
6
8
10
Frequency [Hz]
Simulated (flat)
Simulated (real)
Analytical (flat)

A18

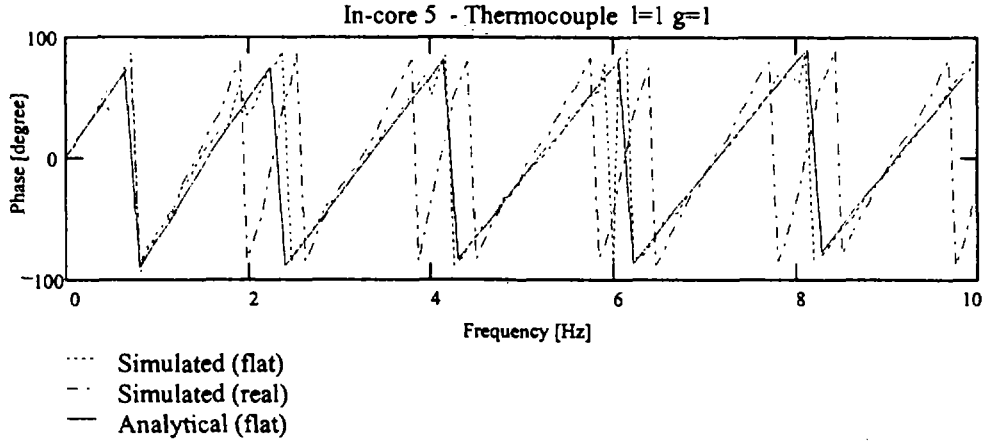
In-core 5 - Thermocouple l=1 g=1
100
0
−100
Phase [degree]
0
2
4
6
8
10
Frequency [Hz]
Simulated (flat)
Simulated (real)
Analytical (flat)

A19

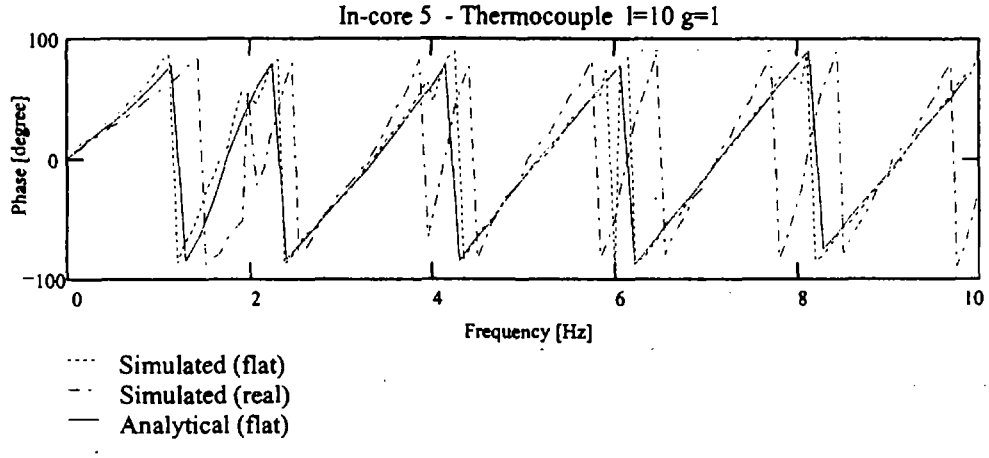
In-core 5 - Thermocouple l=10 g=1
100
0
−100
Phase [degree]
0
2
4
6
8
10
Frequency [Hz]
Simulated (flat)
Simulated (real)
Analytical (flat)

A20

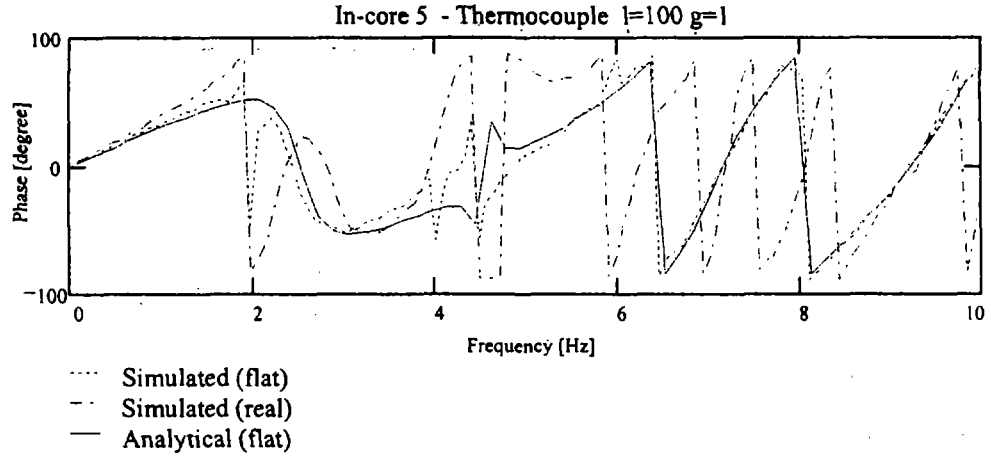
In-core 5 - Thermocouple l=100 g=1
100
0
−100
Phase [degree]
0
2
4
6
8
10
Frequency [Hz]
Simulated (flat)
Simulated (real)
Analytical (flat)

A21

Phase Curves for Inlet Temperature Noise

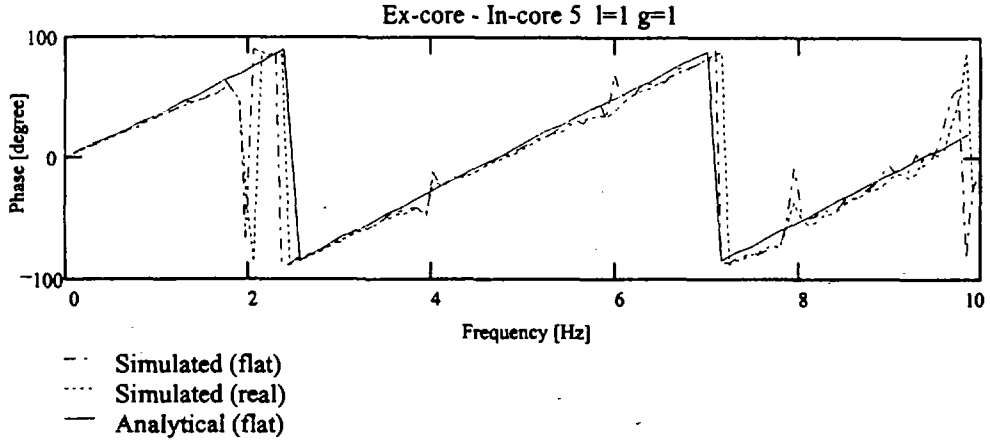

A22

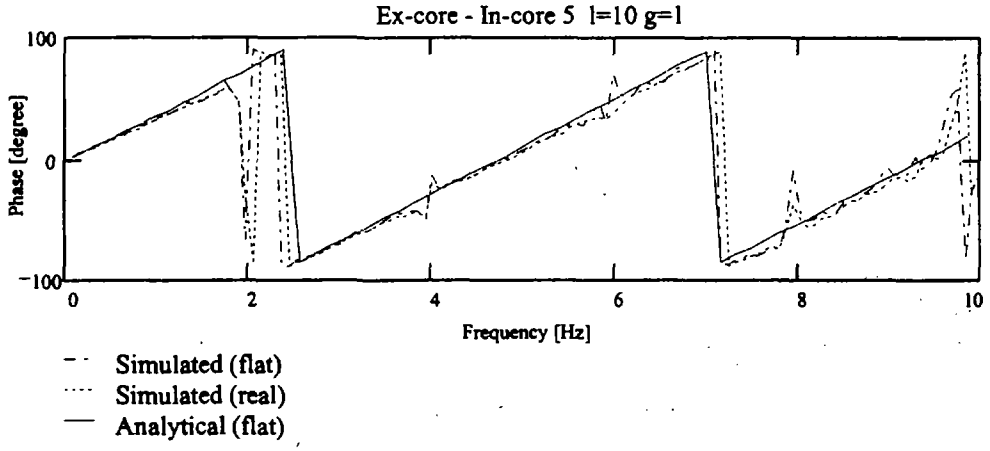

A23

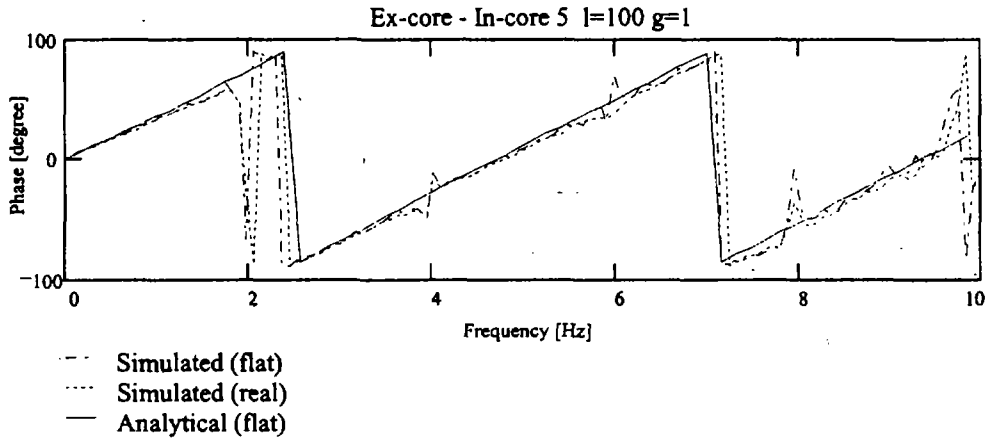

A24

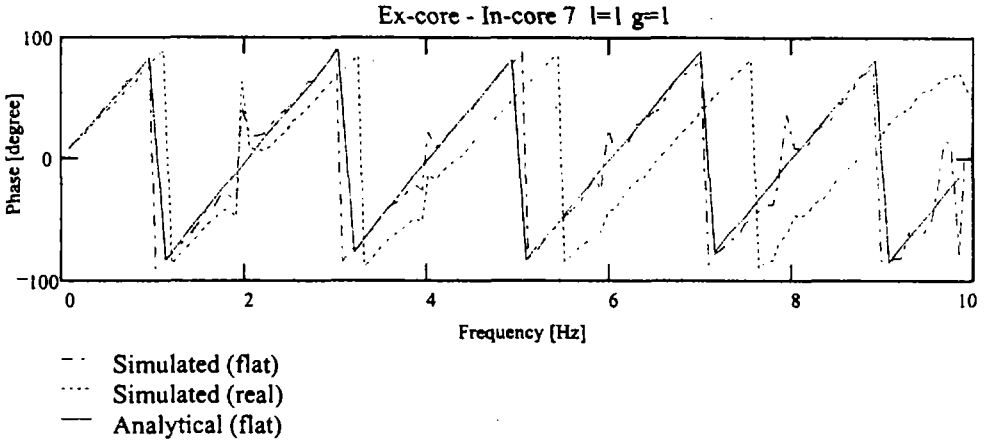
Ex-core - In-core 7 l=1 g=1
100
0
−100
Phase [degree]
0
2
4
6
8
10
Frequency [Hz]
Simulated (flat)
Simulated (real)
Analytical (flat)

A25

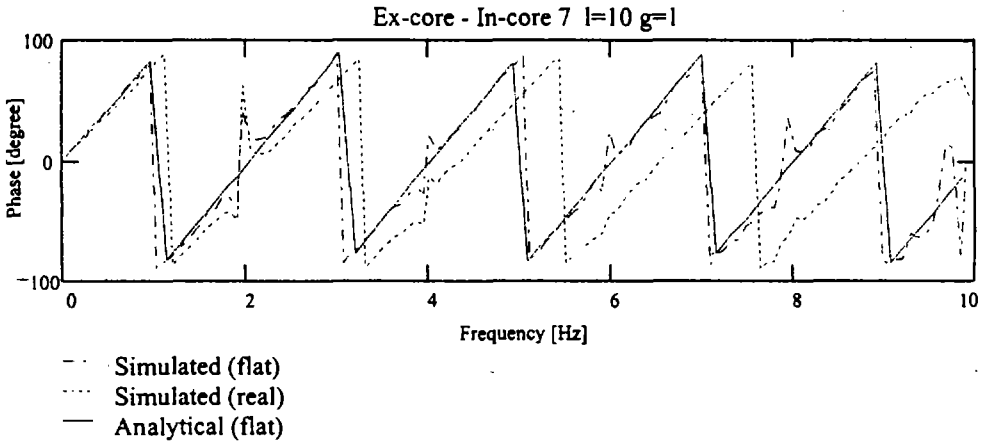
Ex-core - In-core 7 l=10 g=1
100
0
−100
Phase [degree]
0
2
4
6
8
10
Frequency [Hz]
Simulated (flat)
Simulated (real)
Analytical (flat)

A26

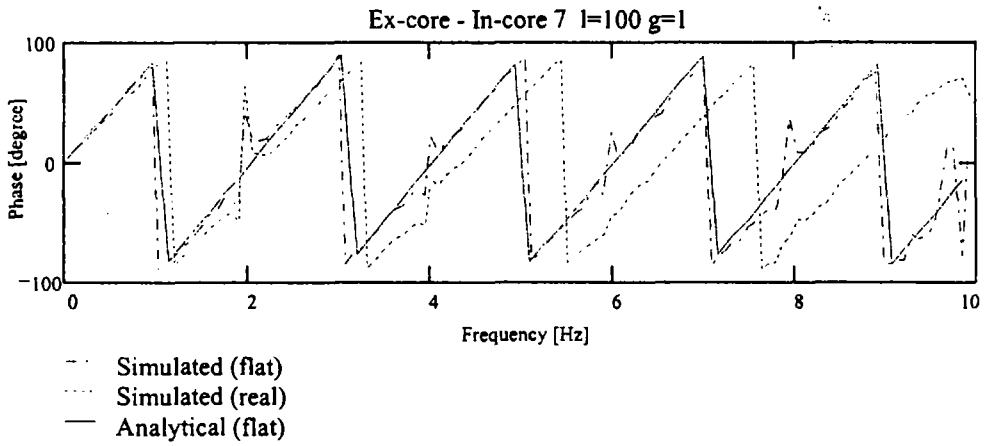
Ex-core - In-core 7 l=100 g=1
100
0
−100
Phase [degree]
0
2
4
6
8
10
Frequency [Hz]
Simulated (flat)
Simulated (real)
Analytical (flat)

A27

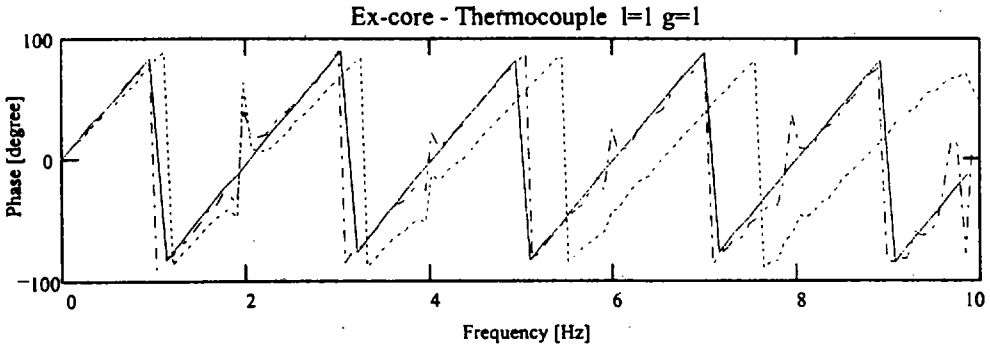
Ex-core - Thermocouple l=1 g=1
Phase [degree]
100
0
−100
0
2
4
6
8
10
Frequency [Hz]
Simulated (flat)
Simulated (real)
Analytical (flat)

A28

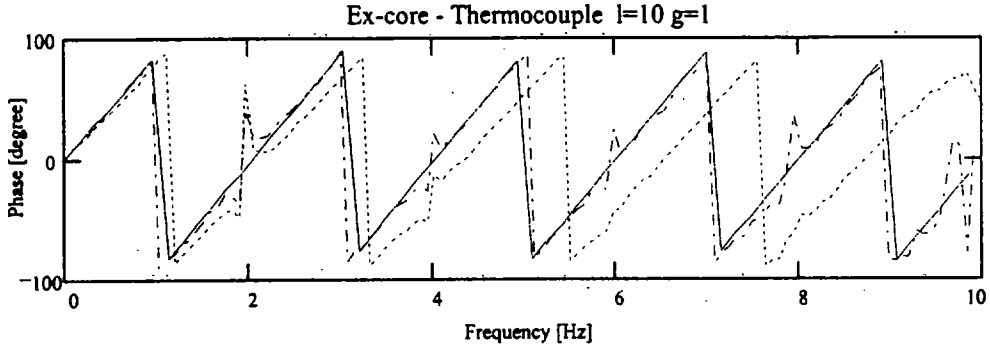
Ex-core - Thermocouple l=10 g=1
Phase [degree]
100
0
−100
0
2
4
6
8
10
Frequency [Hz]
Simulated (flat)
Simulated (real)
Analytical (flat)

A29

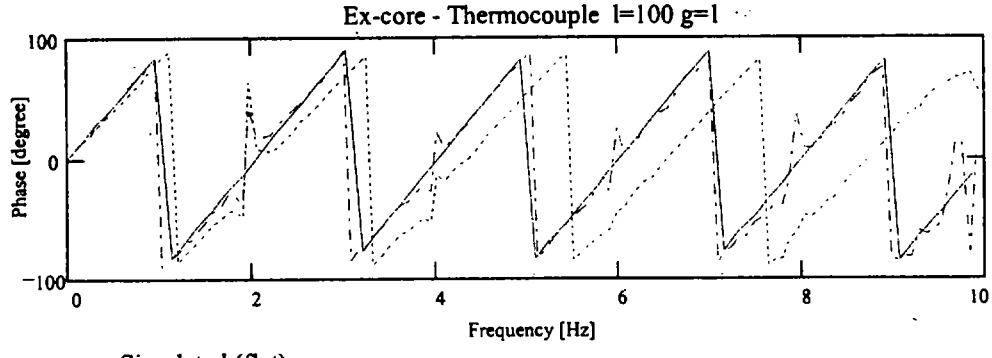
Ex-core - Thermocouple l=100 g=1
Phase [degree]
100
0
−100
0
2
4
6
8
10
Frequency [Hz]
Simulated (flat)
Simulated (real)
Analytical (flat)

A30

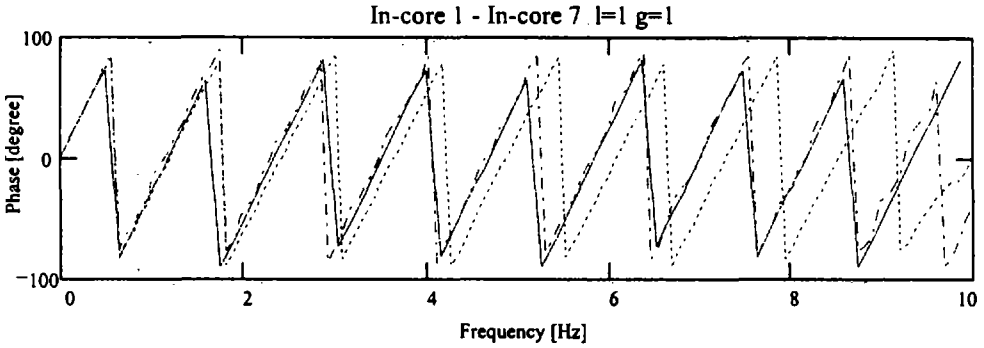
In-core 1 - In-core 7 l=1 g=1
100
0
−100
Phase [degree]
0
2
4
6
8
10
Frequency [Hz]
Simulated (flat)
Simulated (real)
Analytical (flat)

A31

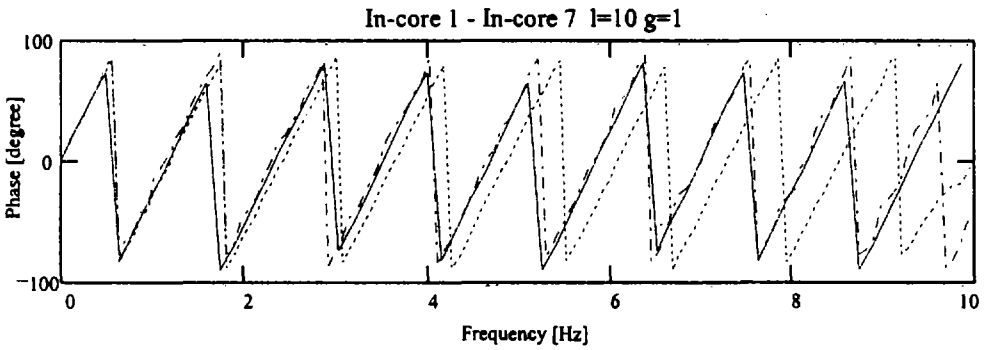
In-core 1 - In-core 7 l=10 g=1
100
0
−100
Phase [degree]
0
2
4
6
8
10
Frequency [Hz]
Simulated (flat)
Simulated (real)
Analytical (flat)

A32

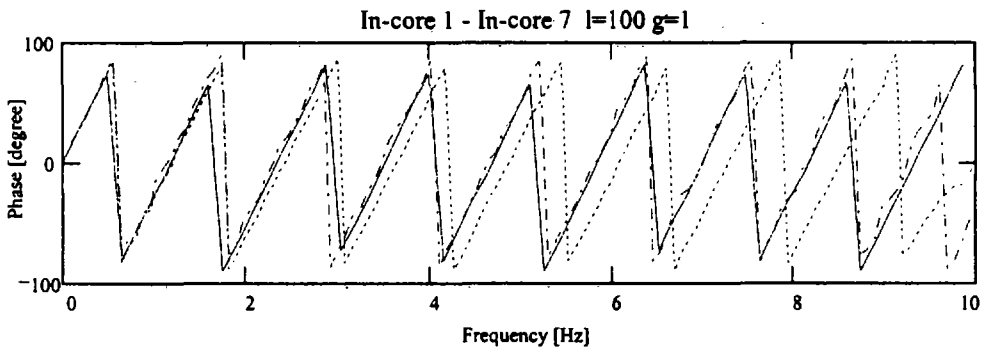
In-core 1 - In-core 7 l=100 g=1
100
0
−100
Phase [degree]
0
2
4
6
8
10
Frequency [Hz]
Simulated (flat)
Simulated (real)
Analytical (flat)

A33

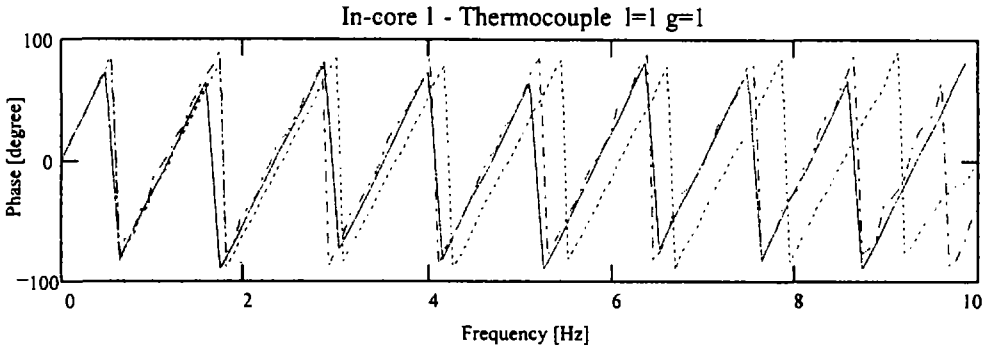
In-core 1 - Thermocouple l=1 g=1
Phase [degree]
100
0
−100
0
2
4
6
8
10
Frequency [Hz]
Simulated (flat)
Simulated (real)
Analytical (flat)

A34

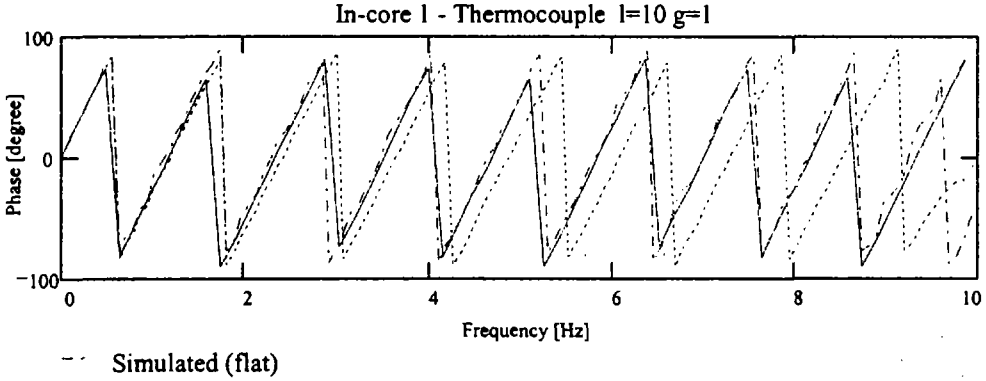
In-core 1 - Thermocouple l=10 g=1
Phase [degree]
100
0
−100
0
2
4
6
8
10
Frequency [Hz]
Simulated (flat)
Simulated (real)
Analytical (flat)

A35

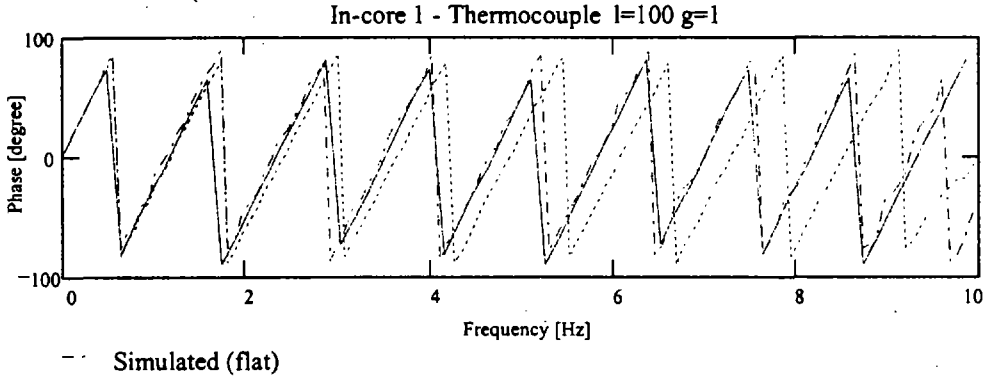
In-core 1 - Thermocouple l=100 g=1
Phase [degree]
100
0
−100
0
2
4
6
8
10
Frequency [Hz]
Simulated (flat)
Simulated (real)
Analytical (flat)

A36

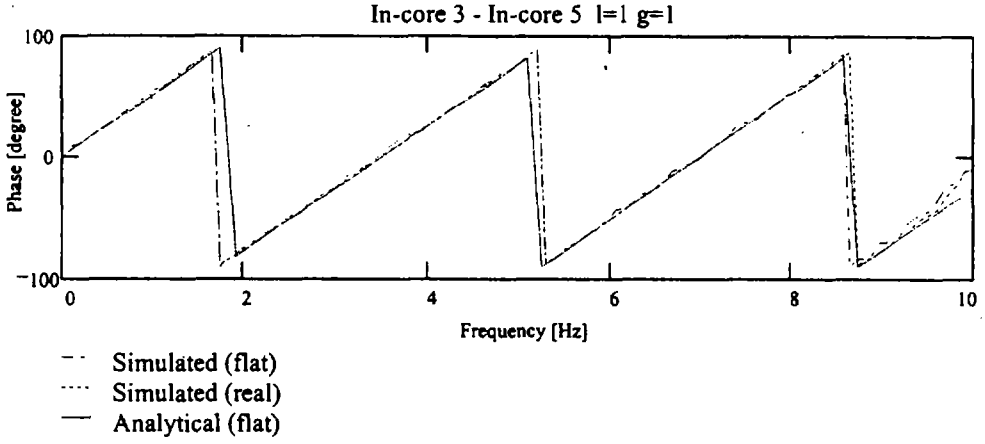
In-core 3 - In-core 5 l=1 g=1
100
0
−100
Phase [degree]
0
2
4
6
8
10
Frequency [Hz]
Simulated (flat)
Simulated (real)
Analytical (flat)

A37

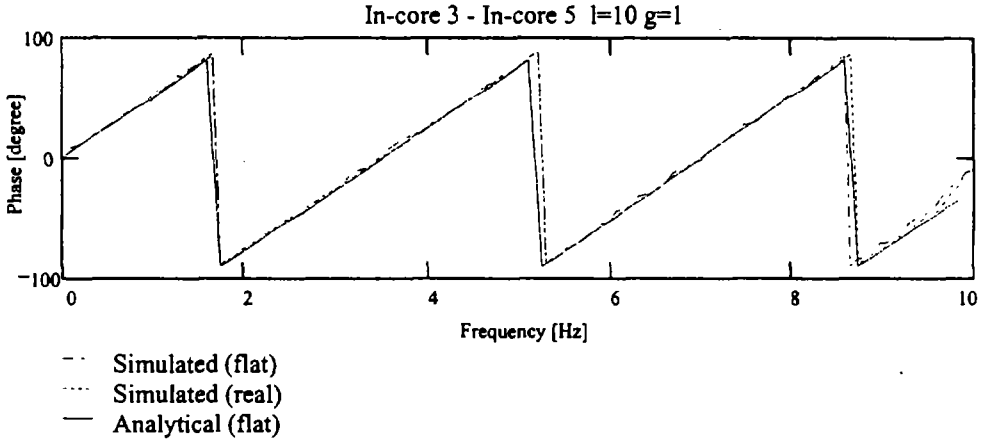
In-core 3 - In-core 5 l=10 g=1
100
0
−100
Phase [degree]
0
2
4
6
8
10
Frequency [Hz]
Simulated (flat)
Simulated (real)
Analytical (flat)

A38

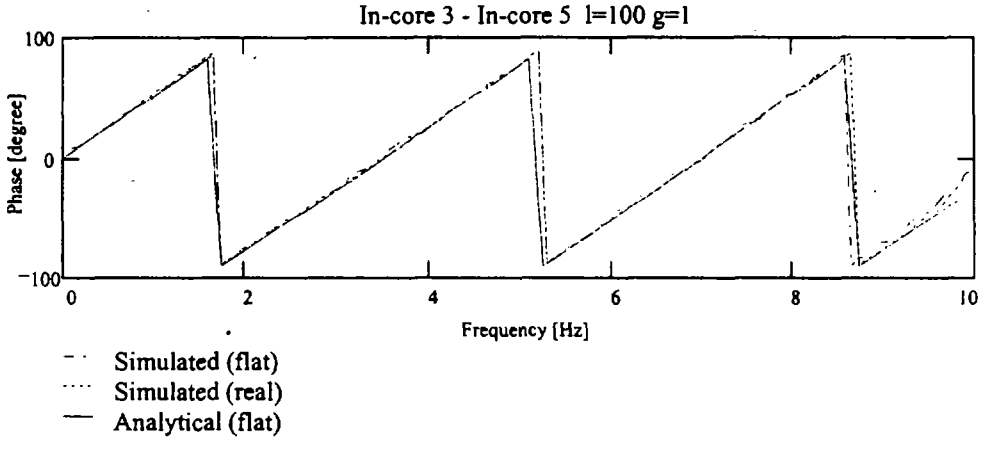
In-core 3 - In-core 5 l=100 g=1
100
0
−100
Phase [degree]
0
2
4
6
8
10
Frequency [Hz]
Simulated (flat)
Simulated (real)
Analytical (flat)

A39

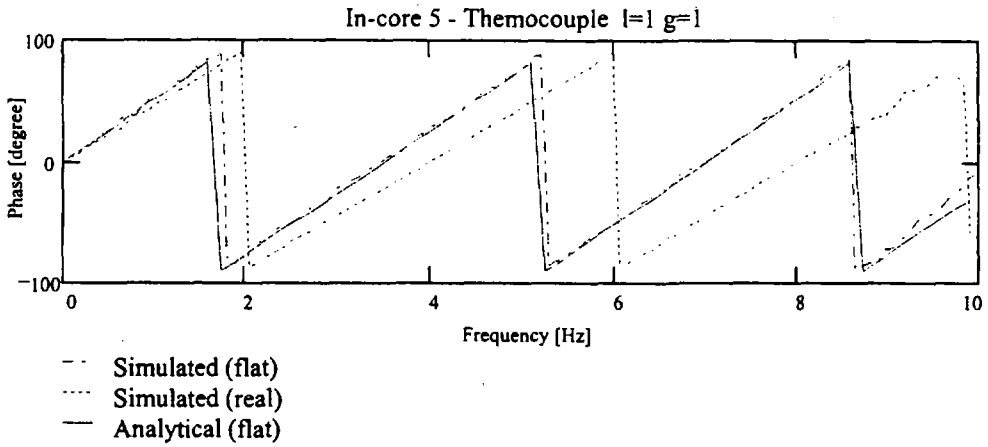
In-core 5 - Themocouple l=1 g=1
100
0
−100
Phase [degree]
0
2
4
6
8
10
Frequency [Hz]
Simulated (flat)
Simulated (real)
Analytical (flat)

A40

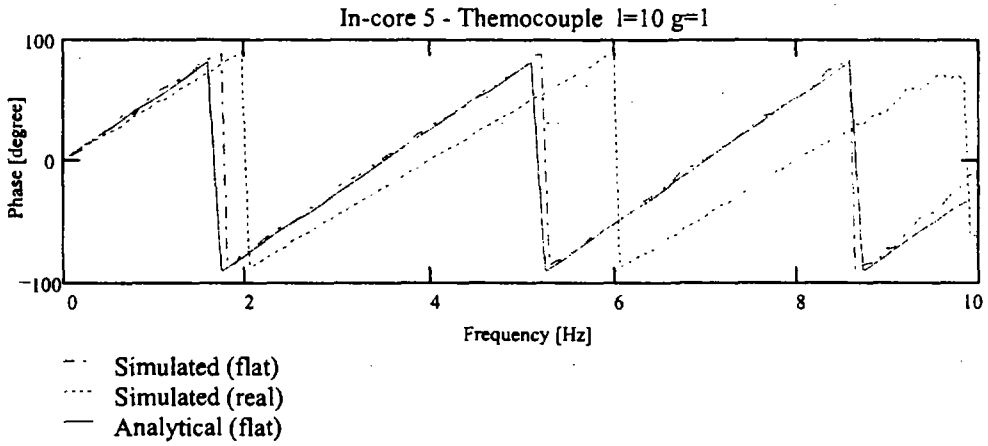
In-core 5 - Themocouple l=10 g=1
100
0
−100
Phase [degree]
0
2
4
6
8
10
Frequency [Hz]
Simulated (flat)
Simulated (real)
Analytical (flat)

A41

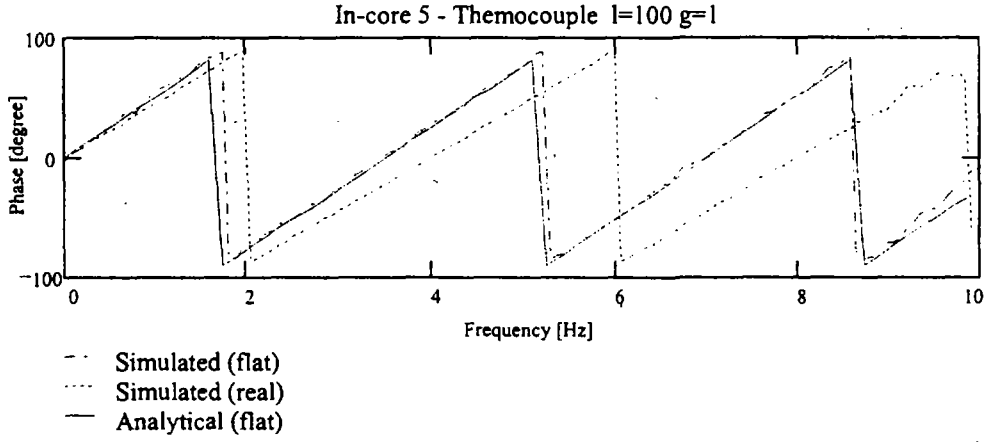
In-core 5 - Themocouple l=100 g=1
100
0
−100
Phase [degree]
0
2
4
6
8
10
Frequency [Hz]
Simulated (flat)
Simulated (real)
Analytical (flat)

A42

Phase Curves for Combinations of Reactivity and Inlet Temperature Noise

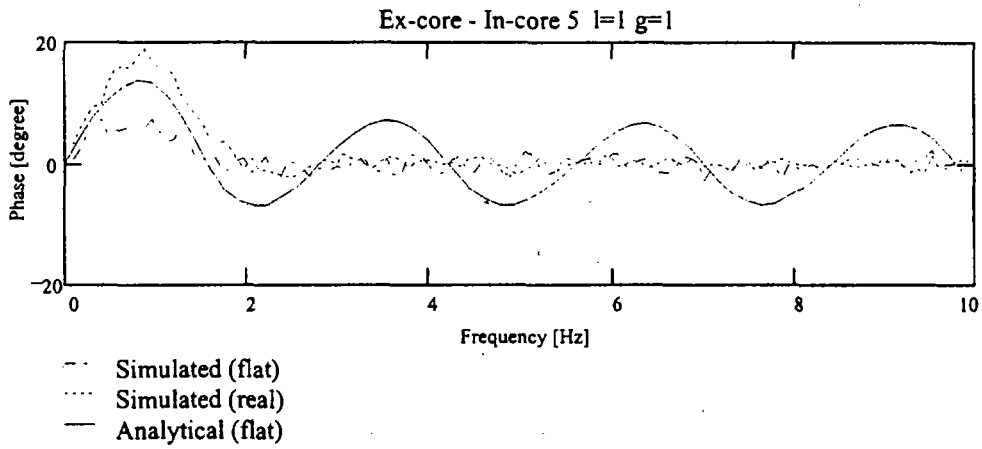

A43

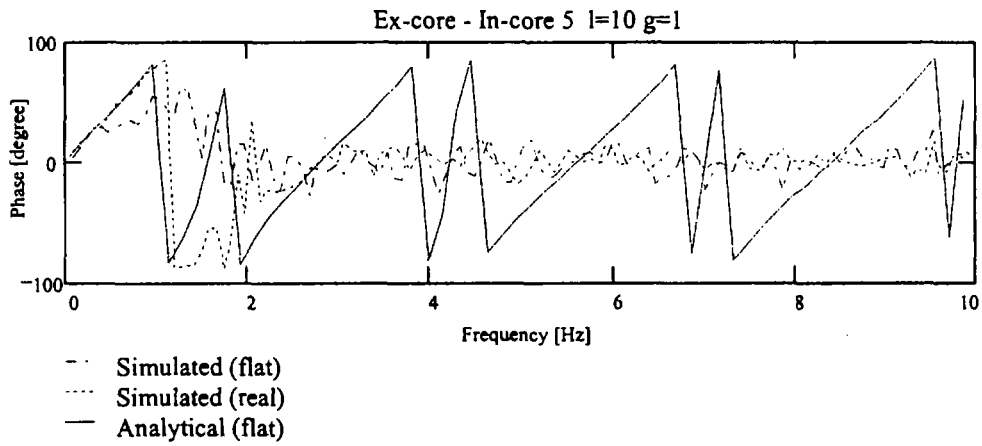

A44

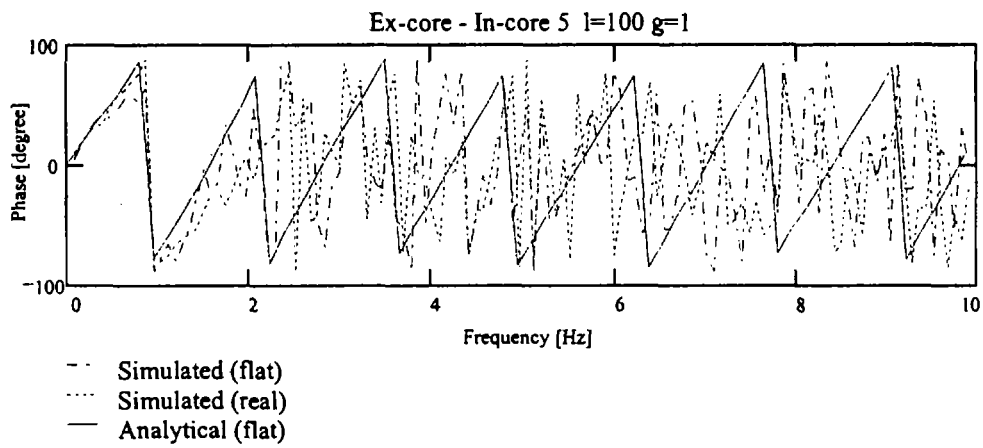

A45

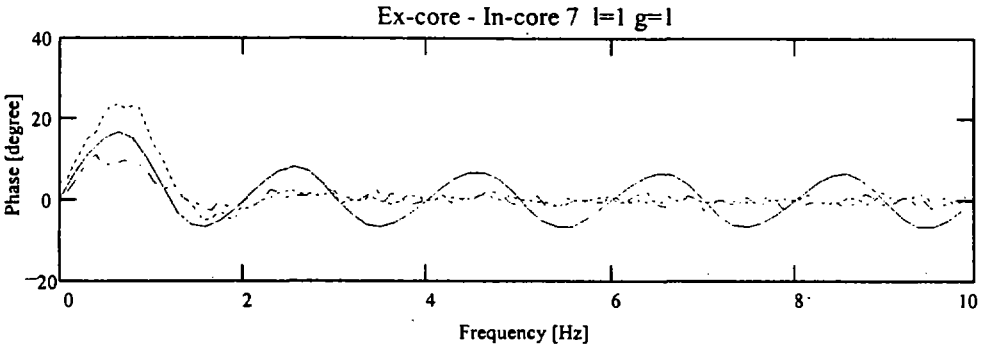
Ex-core - In-core 7 l=1 g=1
Phase [degree]
40
20
0
-20
0
2
4
6
8
10
Frequency [Hz]
Simulated (flat)
Simulated (real)
Analytical (flat)

A46

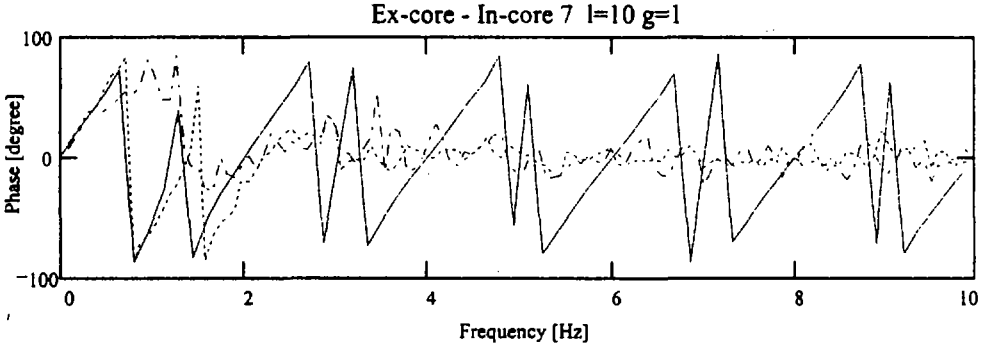
Ex-core - In-core 7 l=10 g=1
Phase [degree]
100
0
-100
0
2
4
6
8
10
Frequency [Hz]
Simulated (flat)
Simulated (real)
Analytical (flat)

A47

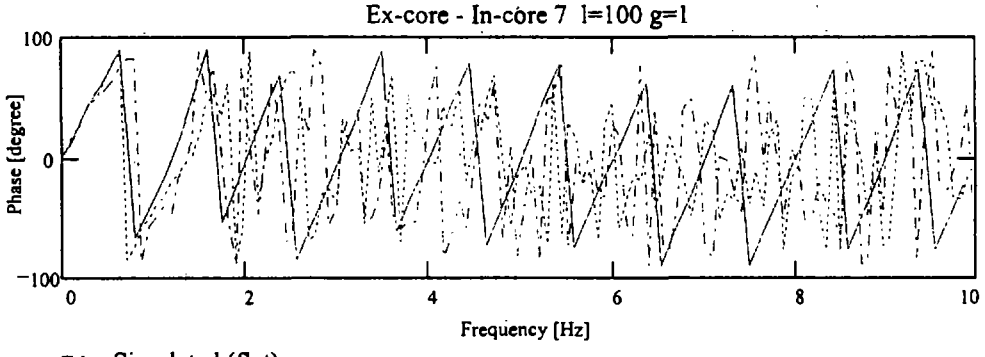
Ex-core - In-core 7 l=100 g=1
Phase [degree]
100
0
-100
0
2
4
6
8
10
Frequency [Hz]
Simulated (flat)
Simulated (real)
Analytical (flat)

A48

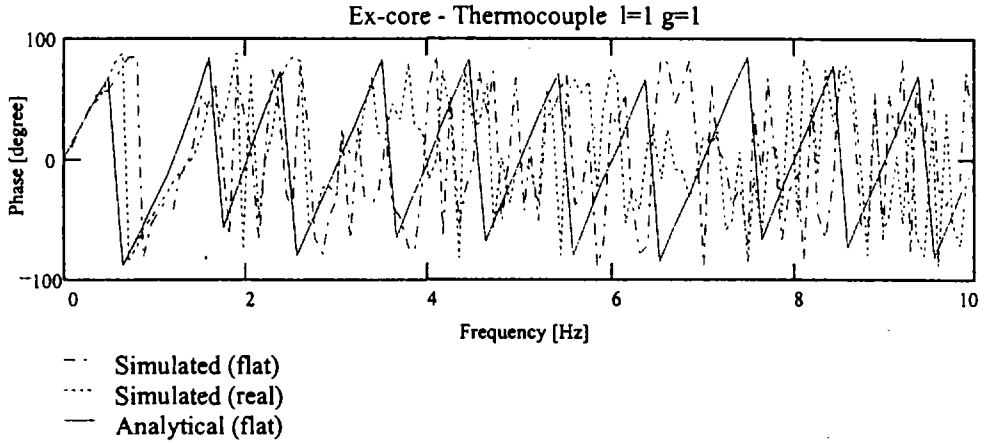
Ex-core - Thermocouple l=1 g=1
Phase [degree]
100
0
−100
0
2
4
6
8
10
Frequency [Hz]
Simulated (flat)
Simulated (real)
Analytical (flat)

A49

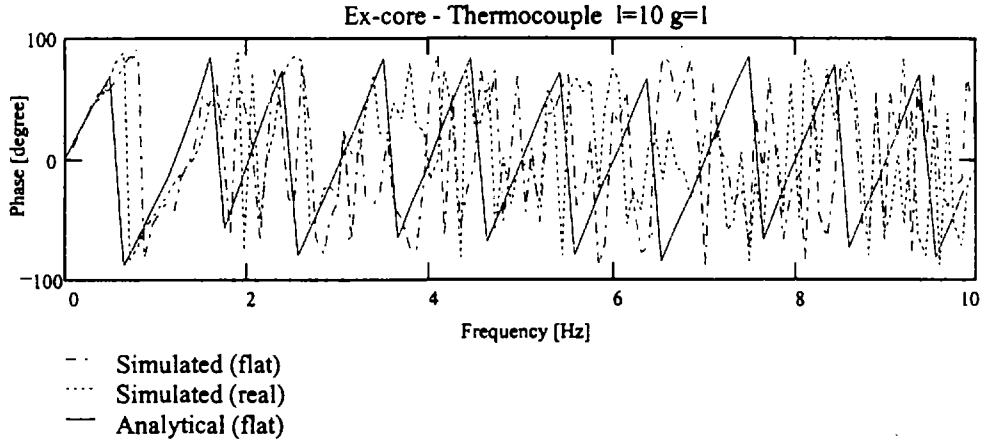
Ex-core - Thermocouple l=10 g=1
Phase [degree]
100
0
−100
0
2
4
6
8
10
Frequency [Hz]
Simulated (flat)
Simulated (real)
Analytical (flat)

A50

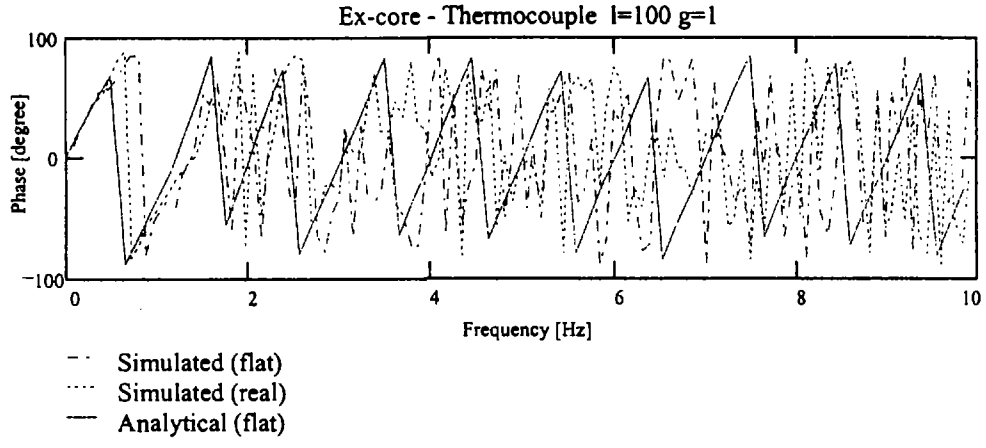
Ex-core - Thermocouple l=100 g=1
Phase [degree]
100
0
−100
0
2
4
6
8
10
Frequency [Hz]
Simulated (flat)
Simulated (real)
Analytical (flat)

A51

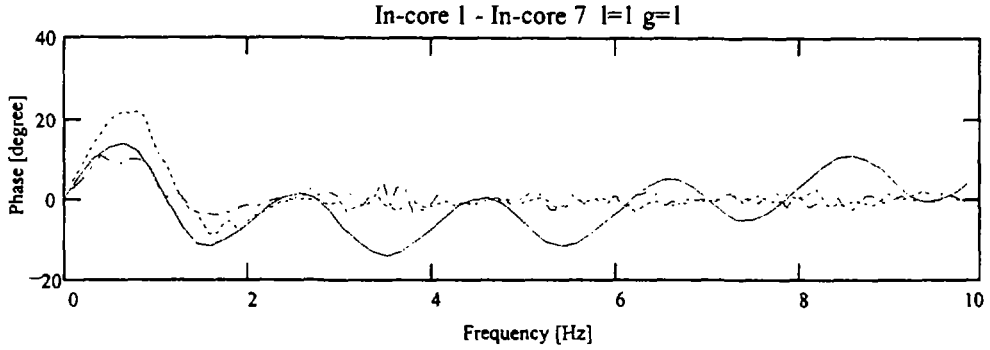
In-core 1 - In-core 7 l=1 g=1
Phase [degree]
40
20
0
-20
0
2
4
6
8
10
Frequency [Hz]
Simulated (flat)
Simulated (real)
Analytical (flat)

A52

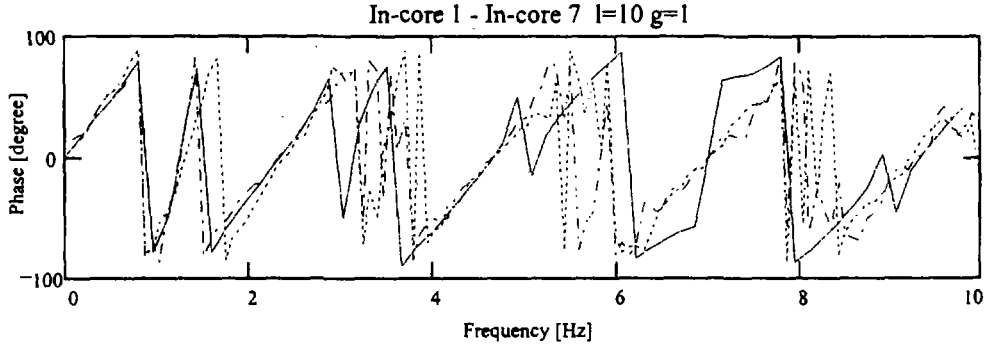
In-core 1 - In-core 7 l=10 g=1
Phase [degree]
100
0
-100
0
2
4
6
8
10
Frequency [Hz]
Simulated (flat)
Simulated (real)
Analytical (flat)

A53

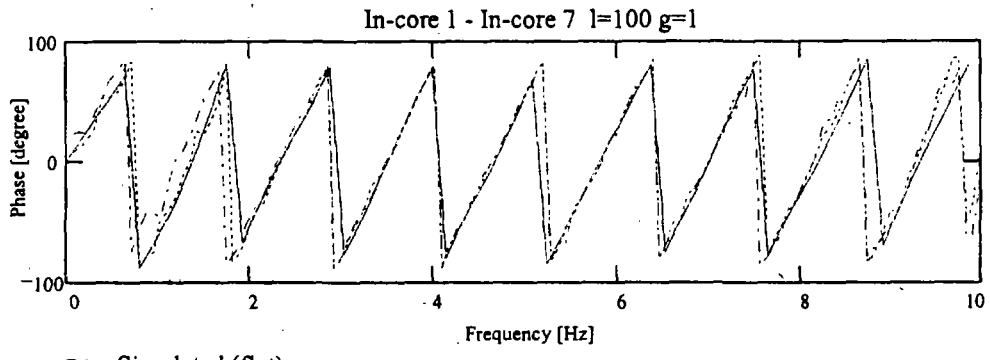
In-core 1 - In-core 7 l=100 g=1
Phase [degree]
100
0
-100
0
2
4
6
8
10
Frequency [Hz]
Simulated (flat)
Simulated (real)
Analytical (flat)

A54

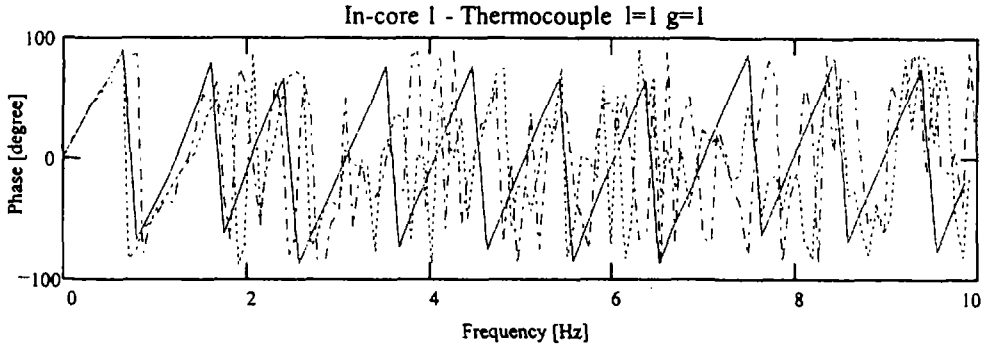
In-core 1 - Thermocouple l=1 g=1
Phase [degree]
100
0
-100
0
2
4
6
8
10
Frequency [Hz]
Simulated (flat)
Simulated (real)
Analytical (flat)

A55

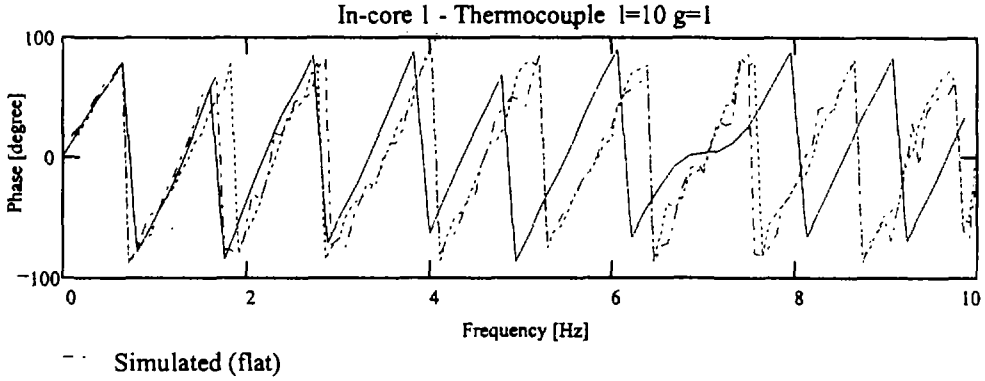
In-core 1 - Thermocouple l=10 g=1
Phase [degree]
100
0
-100
0
2
4
6
8
10
Frequency [Hz]
Simulated (flat)
Simulated (real)
Analytical (flat)

A56

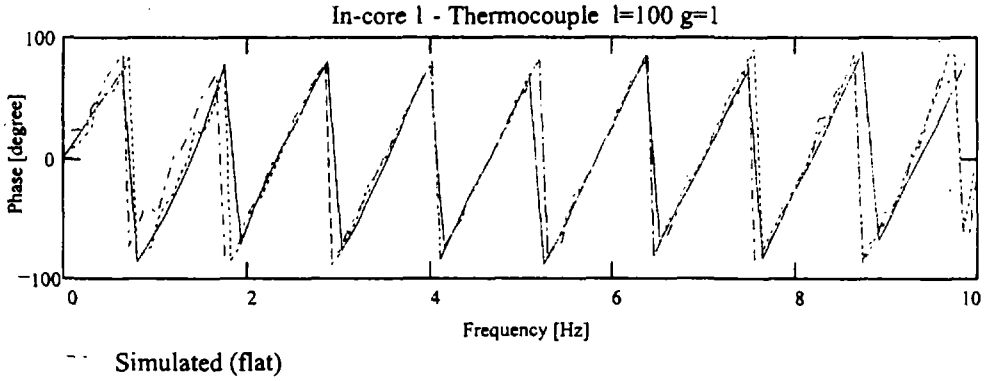
In-core 1 - Thermocouple l=100 g=1
Phase [degree]
100
0
-100
0
2
4
6
8
10
Frequency [Hz]
Simulated (flat)
Simulated (real)
Analytical (flat)

A57

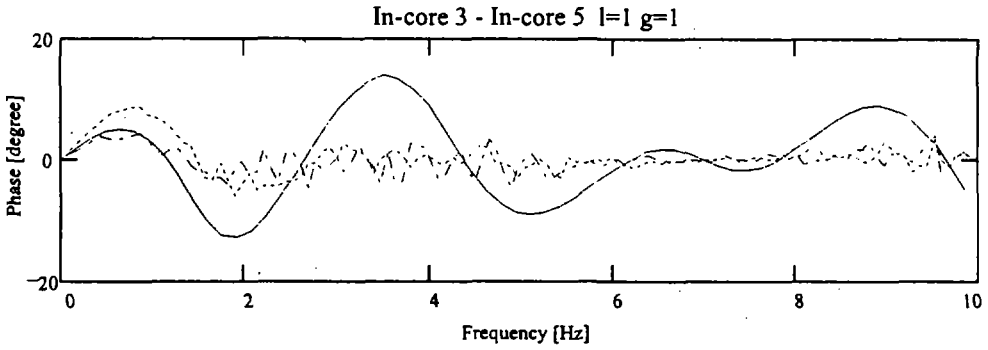

Simulated (flat)
Simulated (real)
Analytical (flat)

A58

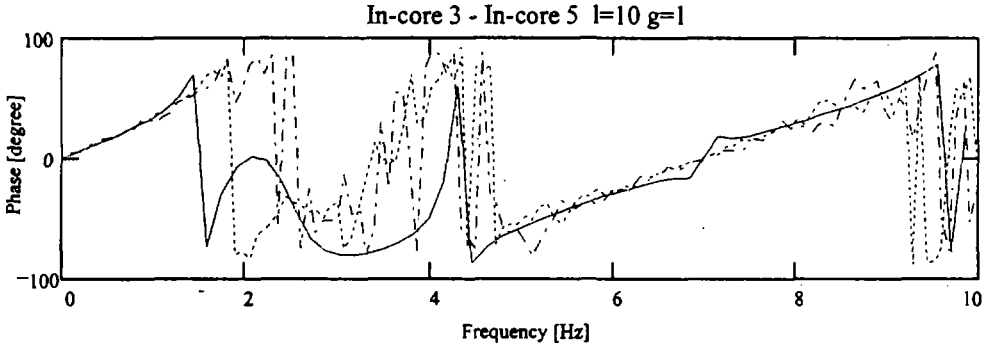

Simulated (flat)
Simulated (real)
Analytical (flat)

A59

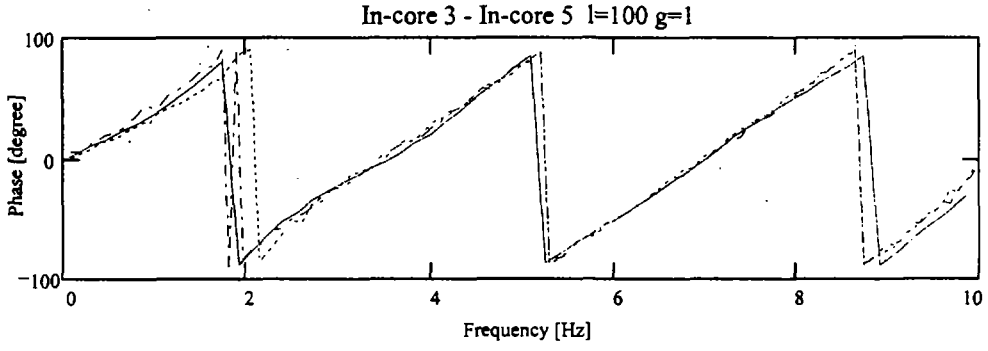

Simulated (flat)
Simulated (real)
Analytical (flat)

A60

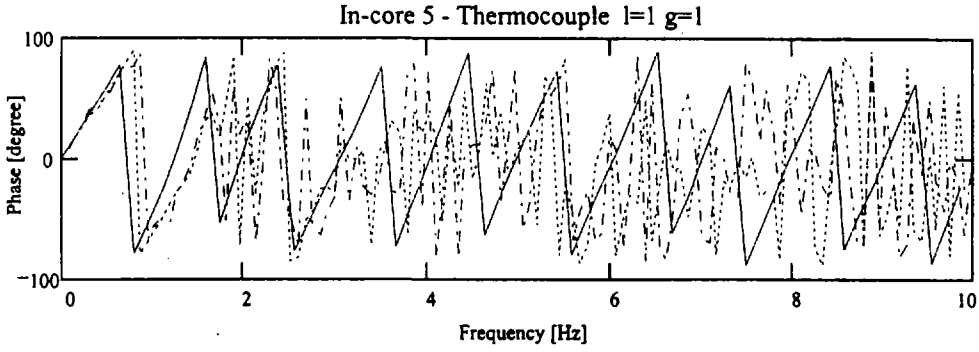
In-core 5 - Thermocouple l=1 g=1
100
0
-100
Phase [degree]
0
2
4
6
8
10
Frequency [Hz]
Simulated (flat)
Simulated (real)
Analytical (flat)

A61

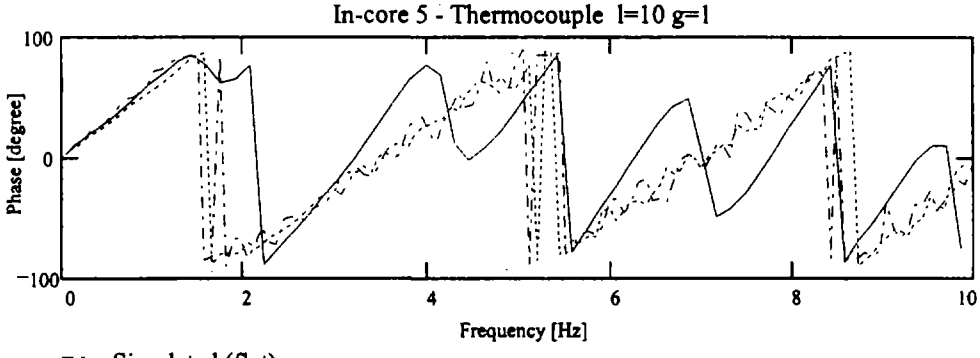
In-core 5 - Thermocouple l=10 g=1
100
0
-100
Phase [degree]
0
2
4
6
8
10
Frequency [Hz]
Simulated (flat)
Simulated (real)
Analytical (flat)

A62

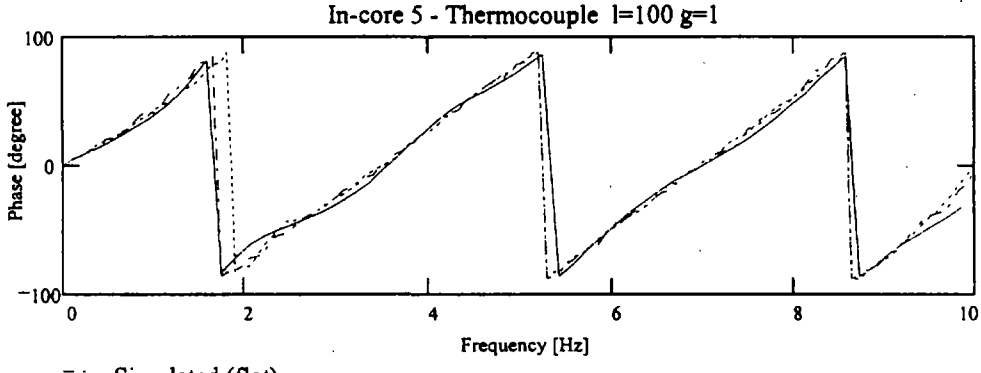
In-core 5 - Thermocouple l=100 g=1
100
0
-100
Phase [degree]
0
2
4
6
8
10
Frequency [Hz]
Simulated (flat)
Simulated (real)
Analytical (flat)

A63

References

[1] **P.E.Kloeden, E.Platen, H. Schurz** *Numerical Solution of SDE Through Computer Experiments* Springer-Verlag, New York, 1994

[2] **R. W. Hamming** *Numerical Methods for Scientists and Engineers.* McGraw-Hill, NewYork, 1962

[3] **D. L. Book** *Finite-Difference Techniques for Vectorized Fluid Dynamics Calculations* Springer-Verlag, New York, 1981

[4] **G.Kosály, Lj.Kostic, L.Miteff,G.Varadi,K.Behringer** *Investigation of the Local Component of the Neutron Noise in a BWR and Its Application to the Study of Two-Phase Flow* Progress in Nuclear Energy Vol. 1, pp. 99-117, 1977

[5] **T.Katona,L.Meskó,G.Pór,J.Valkó** *Some Aspects of the Theory of Neutron Noise Due to Propagating Disturbances* Progress in Nuclear Energy Vol.9, pp. 209-222, 1982

[6] **J. Valkó** *In-Core Generated Temperature Fluctuations and Boiling Detection in Pressurized Water Reactors* Ann. Nucl. Energy Vol. 19, No. 3. pp. 155-168, 1992

[7] **G.Pór** *Investigations on the Phase at Low Frequencies of CPSD between Detectors in the Borselle PWR Power Plant* ECN Report, ECN-81-131, 1981

[8] **D. Lübbesmeyer** *The Influence of a Radial Velocity Profile on the Velocity Measured by Noise Analysis* Ann. Nucl. Energy Vol. 10. No. 8. pp. 421-432, 1983

[9] **G. Kosály** *Noise Investigations in Boiling Water and Pressurized Water Reactors* Progress in Nuclear Energy, Vol. 5, pp. 145-199, 1980

[10] **J.A.Thie** *Power Reactor Noise*, American Nuclear Society , Illinois, 1981

[11] **M.J.J.Hoon** *Investigations on Transport Effects in Pressurized Water Reactors* Thesis, Technical University of Budapest, 1993

[12] **G. Házi, G. Pór** *Behaviour of ODE solvers in the frequency domain*, 1997 (submitted to International Journal of Numerical Methods in Engineering)

[13] **G. Házi, G. Pór** *Numerical Solutions of Ordinary and Partial Differential Equations in the Frequency Domain* KFKI Report, KFKI-1997-02/G, 1997

[14] **G. Házi, G. Pór** *Studies on Linear Phase Formation by Noise Simulator* IMORN-27, Nov. 18-20 Valencia, 1997

[15] **Y. Watanabe** *A Nondispersive and Nondissipative Numerical Method for First-Order Linear Hyperbolic Partial Differential Equations* Numerical Methods for Partial Differential Equations, Vol. 3, pp. 1-8, 1987

The issues of the KFKI preprint/report series are classified as follows:

A. Particle and Nuclear Physics
B. General Relativity and Gravitation
C. Cosmic Rays and Space Research
D. Fusion and Plasma Physics
E. Solid State Physics
F. Semiconductor and Bubble Memory Physics and Technology
G. Nuclear Reactor Physics and Technology
H. Laboratory, Biomedical and Nuclear Reactor Electronics
I. Mechanical, Precision Mechanical and Nuclear Engineering
J. Analytical and Physical Chemistry
K. Health Physics
L. Vibration Analysis, CAD, CAM
M. Hardware and Software Development, Computer Applications, Programming
N. Computer Design, CAMAC, Computer Controlled Measurements

The complete series or issues discussing one or more of the subjects can be ordered; institutions are kindly requested to contact the KFKI Library, individuals the authors.

Title and classification of the issues published this year:

KFKI-1998-01/G *G. Házi, G. Pór:* LINEAR PHASE FORMATION BY NOISE SIMULATOR

Kiadja a Központi Fizikai Kutató Intézet
Felelős kiadó: Házi Gábor
Készítette: Prosperitás Nyomdaipari Kft
Példányszám: 147
Budapest, 1998. január hó